Journal of Computational Physics **181,** 126–154 (2002)
doi:10.1006/jcph.2002.7091

Coupling of Fast Multipole Method and Microlocal Discretization for the 3-D Helmholtz Equation

Eric Darrigrand

CEA/CESTA-MAB-LRC-M03, B.P.2, 33114 Le Barp, France; and Université Bordeaux 1, Mathématiques Appliquées, 351 cours de la Libération, 33405 Talence Cedex, France
E-mail: Eric.Darrigrand@math.u-bordeaux.fr

Received September 7, 2001; revised April 17, 2002

We are concerned with an integral method applied to the solution of the Helmholtz equation where the linear system is solved using an iterative method. We need to perform matrix–vector products whose time and memory requirements increase as a function of the wavenumber κ. Many methods have been developed to speed up the matrix–vector product calculation or to reduce the size of the system. Microlocal discretization methods enable one to consider new systems with reduced size. Another method, the fast multipole method, is one of the most efficient and robust methods used to speed up the calculation of matrix–vector products. In this paper, a coupling of these two recently developed methods is presented. This coupling enables one to reduce CPU time very efficiently for large wavenumbers. Satisfactory numerical tests are also presented to confirm the theoretical study within a new integral formulation. Results are obtained for a sphere with a size of 26λ using a resolution based on a mesh with an average edge length of about 2λ, where λ is the wavelength. Results are also given for an industrial test case from Dassault–Aviation, the Cetaf.

Key Words: Helmholtz; integral equation; finite element; fast multipole method; microlocal discretization.

1. INTRODUCTION

A numerical solution to the boundary integral equation for the exterior Helmholtz problem in three dimensions leads to the solution of a dense linear system. In order to have a well-conditioned system, we consider new integral equations written by B. Després. Després and co-workers [16, 32; see also 5, 31] wrote new integral equations with properties that enable one to use an iterative solution based on the conjugate gradient.

0021-9991/02 $35.00

In order to accelerate the iterative solution of the system, we have considered a coupling of two methods, the microlocal discretization method and the fast multipole method (FMM).

Under particular conditions, the microlocal discretization method, according to Abboud *et al.* [1, 2] consists of approximating the phase of the unknown using the geometrical optics method. Consequently, the oscillation of the new unknown is reduced. We can then consider a numerical approximation with a number of degrees of freedom N_d clearly less, according to the wavenumber κ. Indeed, in the classical case we have $N_d \sim \kappa^2$, while $N_d \sim \kappa^{2/3}$ after approximation of the phase. Nevertheless, the discretization of the geometry implies a consideration of $\mathcal{O}(N)$ elements, with $N \sim \kappa^2$, on the surface of the obstacle. Then, the calculation of the matrix of the system also needs $\mathcal{O}(N^2)$ operations with $N \sim \kappa^2$, as in the classical case. Thus, the authors of the method suggested the use of the theory of the stationary phase in order to accelerate the calculation of the matrix [2, 19]. However, this theory does not enable one to have a good estimate of the CPU time needed for good accuracy, and the extension to the 3-D case implies difficulties not yet solved. de la Bourdonnaye has given another version of the microlocal discretization method [14, 15], which also makes use of the stationary-phase theory.

The FMM is based on another idea. The issue is to factorize the product $A \cdot Y$ and to cluster advisedly the terms in order to reduce both resolution time and memory requirement. From the geometrical point of view, the calculus of far interactions is greatly speeded up by clustering the elements of the mesh properly. The one-level FMM (respectively multilevel FMM) results in an algorithm of complexity $\mathcal{O}(N^{3/2})$ (respectively $\mathcal{O}(N \ln^2 N)$), where $N \sim \kappa^2$. This method introduced for the Laplace equation by Greengard and Rokhlin [17, 18] was extended for the Helmholtz and Maxwell equations by Rokhlin [26, 27], Chew and co-workers [7, 20, 28–30, 34], Darve [11–13], and other [8, 25].

The object of this paper is to describe a coupling of the microlocal discretization method according to Abboud *et al.* and the one-level FMM. The ideas of this work have briefly been presented at conferences [9, 10]. Using the approximation of the phase of the unknown, the microlocal discretization method enables one to consider a numerical approximation with a number of degrees of freedom $\mathcal{O}(\kappa^{2/3})$ instead of $\mathcal{O}(\kappa^2)$, as in the classical case. The size of the system is then $\mathcal{O}(\kappa^{2/3} \times \kappa^{2/3})$. Nevertheless, due to geometrical approximations, the matrix calculation still requires $\mathcal{O}(\kappa^2 \times \kappa^2)$ operations. In this paper we suggest using the one-level FMM in order to speed up the matrix calculation instead of the use of the theory of the stationary phase. This is a different use of the FMM since in our method the matrix of the system is calculated once and stored, and the FMM is used to accelerate its calculation. Thus, the matrix calculation is performed due to an algorithm with complexity κ^3 instead of κ^4. We also did a theoretical study of the use of a multilevel FMM. This should enable one to obtain a matrix calculation with complexity $\kappa^{8/3}$. This idea will be the topic of another paper.

First, we present the new integral equations and the classical solution of this system. Next, we present the microlocal discretization method and the FMM in order to give a comprehensive theoretical study of our coupling of the methods. Finally, numerical tests are considered to confirm the theoretical study. The scattering of the unit sphere is studied for large frequencies (up to a size of 26λ and an area of $2100\lambda^2$ for the sphere, with a coarse mesh whose average edge length is 2λ, where λ is the wavelength), and an industrial test case from Dassault–Aviation, called the CETAF and presented by Darve [13], is considered.

General notations are as follows:

ι	$\sqrt{-1}$
λ	wavelength
κ	wavenumber $\kappa = 2\pi/\lambda$
j_m	spherical Bessel function
y_m	spherical Neumann function
$h_m^{(1)}$	spherical Hankel function of the first kind, $h_m^{(1)} = j_m + \iota y_m$
P_m	Legendre polynomial
S^2	unit sphere $S^2 = \{\hat{s} \in \mathbb{R}^3/|\hat{s}| = 1\}$

2. NEW INTEGRAL EQUATIONS FOR THE 3-D HELMHOLTZ PROBLEM

2.1. Formulation of the New Integral Equations

Després wrote a new system of integral equations for the 3-D Maxwell equation and the 2-D Helmholtz equation. This system derives from the minimization of a quadratic functional. Classical systems do not have good matrix properties and are not suitable for an efficient iterative resolution. On the other hand, the considered IE (new integral equations, according to Després) lead to a new system whose matrix properties enable one to use an efficient iterative resolution based on the conjugate gradient without the use of preconditioning. Thus, in this paper, we study the coupling of the microlocal discretization and the fast multipole method for the solution of this IE system. However, this coupling could be considered in the same way for more classical integral systems. Bartoli and Collino rewrote the IE for the 2-D Helmholtz equation in a more comprehensible way (see [5]). In this section, we establish the IE for the 3-D Helmholtz equation in a way similar to that of N. Bartoli and F. Collino.

We first consider the Helmholtz equation with the particular impedance boundary condition

$$\begin{cases} \Delta u + \kappa^2 u = 0 & \text{in } \Omega^+, \\ \frac{\partial u}{\partial n}_{/\Gamma} + \iota\kappa u_{/\Gamma} = g & \text{on } \Gamma, \\ \lim\limits_{r\to+\infty} r\left(\frac{\partial u}{\partial r} - \iota\kappa u\right) = 0, \end{cases} \tag{1}$$

where Ω^- is a regular bounded domain of $\mathbb{R}^3$, of boundary Γ, and $\Omega^+ = \mathbb{R}^3\backslash\overline{\Omega^-}$ (Fig. 1). g is given as a function of the incident wave. The unit normal n is directed to the exterior domain.

A first equation is obtained, considering that the solution of

$$\begin{cases} \Delta u + \kappa^2 u = 0 & \text{in } \Omega^+ \\ \lim\limits_{r\to+\infty} r\left(\frac{\partial u}{\partial r} - \iota\kappa u\right) = 0 \end{cases}$$

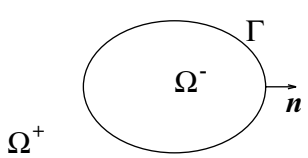

FIG. 1. The obstacle.

is given by

$$\kappa u = M\big(\kappa u_{/\Gamma}\big) - L\left(\frac{\partial u}{\partial n}{}_{/\Gamma}\right) \quad \text{in } \Omega^+. \tag{2}$$

L and M are the single- and double-layer potential defined for all x not in Γ by

$$Lp(x) = \kappa \int_\Gamma G(x,y)p(y)\,d\gamma(y) \quad \text{and} \quad M\varphi(x) = \int_\Gamma \frac{\partial G}{\partial n_y}(x,y)\varphi(y)\,d\gamma(y),$$

with $G(x,y) = \frac{e^{\iota\kappa|x-y|}}{4\pi|x-y|}$.

With the notations $q = \kappa u_{/\Gamma}$ and $p = \frac{\partial u}{\partial n}{}_{/\Gamma}$, we have the relations

$$\begin{bmatrix} D & -K' - \frac{I}{2} \\ -K + \frac{I}{2} & S \end{bmatrix} \begin{bmatrix} q \\ p \end{bmatrix} = \begin{bmatrix} 0 \\ 0 \end{bmatrix}, \tag{3}$$

where the operators S, K, K', and D are defined for all x in Γ by

$$Sp(x) = \kappa \int_\Gamma G(x,y)\,p(y)\,d\gamma(y), \quad Dq(x) = \frac{1}{\kappa}\int_\Gamma \frac{\partial^2 G}{\partial n_x \partial n_y}(x,y)\,q(y)\,d\gamma(y),$$
$$Kq(x) = \int_\Gamma \frac{\partial G}{\partial n_y}(x,y)\,q(y)\,d\gamma(y), \quad K'p(x) = \int_\Gamma \frac{\partial G}{\partial n_x}(x,y)\,p(y)\,d\gamma(y).$$

The singularity of D will be treated by the formula

$$\langle Dq, q'\rangle_{L^2(\Gamma)} = \frac{1}{\kappa}\int_\Gamma\int_\Gamma G(x,y)[\kappa^2 q(y)\,\overline{q'(x)}(n_x\cdot n_y)$$
$$- \overrightarrow{\operatorname{curl}}_\Gamma q(y)\cdot \overrightarrow{\operatorname{curl}}_\Gamma \overline{q'(x)}]\,d\gamma(y)\,d\gamma(x).$$

Considering the kernel expression, two other relations can be derived from the system (3). The kernel $G(x,y)$ can be split into real and imaginery parts

$$G(x,y) = G_r(x,y) + \iota G_i(x,y), \quad \text{with} \begin{cases} G_r(x,y) = \frac{\cos(\kappa|x-y|)}{4\pi|x-y|}, \\ G_i(x,y) = \frac{\sin(\kappa|x-y|)}{4\pi|x-y|}. \end{cases} \tag{4}$$

Following this decomposition, the operators read

$$S = S_r + \iota S_i, \quad K = K_r + \iota K_i, \quad K' = K'_r + \iota K'_i, \quad D = D_r + \iota D_i,$$

where S_r, K_r, K'_r, D_r, S_i, K_i, K'_i, and D_i are real operators.

We now introduce a new couple of unknowns on the boundary, $\mu = \iota q$ and $\lambda = \iota p$. Thus, system (3) becomes

$$\mathbf{K}\begin{bmatrix} q \\ p \end{bmatrix} + \mathbf{M}\begin{bmatrix} \mu \\ \lambda \end{bmatrix} = \begin{bmatrix} 0 \\ 0 \end{bmatrix}, \tag{5}$$

where

$$\mathbf{K} = \begin{bmatrix} D_r & -K_r' - \frac{I}{2} \\ -K_r + \frac{I}{2} & S_r \end{bmatrix} \quad \text{and} \quad \mathbf{M} = \begin{bmatrix} D_i & -K_i' \\ -K_i & S_i \end{bmatrix},$$

which implies, multiplying by ι,

$$\mathbf{K}\begin{bmatrix} \mu \\ \lambda \end{bmatrix} = \mathbf{M}\begin{bmatrix} q \\ p \end{bmatrix}. \tag{6}$$

S_r and D_r are symmetrical, and $\mathbf{K}$ is related to its adjoint $\mathbf{K}^*$ through the relation

$$\mathbf{K} - \mathbf{K}^* = \begin{bmatrix} 0 & -I \\ I & 0 \end{bmatrix} = \Pi. \tag{7}$$

Up to now, the boundary condition has not been used. It implies the two equivalent relations

$$p + \mu = g,$$
$$-\lambda + q = -\iota g.$$

Letting $\tilde{g} = \left[\begin{smallmatrix} -\iota g \\ g \end{smallmatrix}\right]$, we obtain

$$\begin{bmatrix} q \\ p \end{bmatrix} + \Pi\begin{bmatrix} \mu \\ \lambda \end{bmatrix} = \tilde{g}. \tag{8}$$

Hence, considering relations (6)–(8), we obtain the system

$$\begin{bmatrix} q \\ p \end{bmatrix} + \mathbf{M}\begin{bmatrix} q \\ p \end{bmatrix} - \mathbf{K}^*\begin{bmatrix} \mu \\ \lambda \end{bmatrix} = \tilde{g}. \tag{9}$$

We now proceed to the derivation of the matrix $\mathbf{M}$ from the far field operator in order to deduce some of its properties. Let us consider the operator defined for all p, q in $L^2(\Gamma)$ and $\hat{s}$ in S^2:

$$\left(A_\infty\begin{bmatrix} q \\ p \end{bmatrix}\right)(\hat{s}) = \frac{\kappa}{4\pi}\int_\Gamma e^{-\iota\kappa y\cdot\hat{s}}\cdot(p(y) + \iota(\hat{s}\cdot n_y)q(y))\,d\gamma(y). \tag{10}$$

Its adjoint is given for all φ in $L^2(S^2)$ by

$$(A_\infty^*\varphi)(y) = \begin{bmatrix} \frac{-\kappa}{4\pi}\int_{S^2}\iota(\hat{s}\cdot n_y)e^{\iota\kappa y\cdot\hat{s}}\varphi(\hat{s})\,d\hat{s} \\ \frac{\kappa}{4\pi}\int_{S^2} e^{\iota\kappa y\cdot\hat{s}}\varphi(\hat{s})\,d\hat{s} \end{bmatrix}, \tag{11}$$

where $\int_{S^2}\cdot\,d\hat{s}$ denotes the integral around the unit sphere S^2. Next, using the relation

$$\frac{\sin(\kappa|x-y|)}{4\pi|x-y|} = \frac{\kappa}{(4\pi)^2}\int_{S^2} e^{\iota\kappa(x-y)\cdot\hat{s}}\,d\hat{s},$$

we can easily check that

$$\mathbf{M} = A_\infty^* A_\infty; \tag{12}$$

i.e., for all $p, q \in L^2(\Gamma)$,

$$\int_{S^2} A_\infty \begin{bmatrix} q \\ p \end{bmatrix} . \overline{A_\infty \begin{bmatrix} \tilde{q} \\ \tilde{p} \end{bmatrix}} d\hat{s} = \int_\Gamma \left(\mathbf{M} \begin{bmatrix} q \\ p \end{bmatrix} \right) \cdot \overline{\begin{bmatrix} \tilde{q} \\ \tilde{p} \end{bmatrix}} d\Gamma. \tag{13}$$

Considering relations (5) and (9), we obtain the system

$$\begin{cases} X + A_\infty^* A_\infty X - \mathbf{K}^* Y = \tilde{g}, \\ \mathbf{K} X + A_\infty^* A_\infty Y = 0, \end{cases} \tag{14}$$

where $X = \left[\begin{smallmatrix} q \\ p \end{smallmatrix} \right]$ and $Y = \imath X = \left[\begin{smallmatrix} \mu \\ \lambda \end{smallmatrix} \right]$. The theory of the inf–sup condition enables one to check the existence and the unicity of X and the existence of Y. In order to gain the unicity of Y, B, Després suggested the modification (see [5]) of adding

$$\begin{aligned} &\beta X = -\imath \beta Y \quad \text{to the first equation} \\ \text{and} \quad &\beta Y = \imath \beta X \quad \text{to the second one,} \end{aligned} \tag{15}$$

given that β is a strictly positive parameter. We then obtain the β-system

$$\begin{cases} (Id + \beta) X + A_\infty^* A_\infty X - \mathbf{K}^* Y = \tilde{g} - \imath \beta Y, \\ \mathbf{K} X + (\beta + A_\infty^* A_\infty) Y = \imath \beta X. \end{cases} \tag{16}$$

Hence, with the coercivity condition satisfied, the β-system has a unique solution (X, Y), and this solution satisfies

$$Y = \imath X. \tag{17}$$

Now, consider a general impedance condition, the Robin condition

$$\frac{\partial u}{\partial n}_{/\Gamma} + \imath \kappa Z u_{/\Gamma} = f \text{ on } \Gamma,$$

where the impedance operator Z has a positive real part. The Dirichlet condition can be considered when $Z \to +\infty$. Let R be the associated reflection operator

$$R = \frac{Id - Z}{Id + Z}.$$

This condition is written in the form

$$\frac{\partial u}{\partial n}_{/\Gamma} + \imath \kappa u_{/\Gamma} = g \quad \text{on } \Gamma,$$

with g expressed as

$$g = R\left(-\frac{\partial u}{\partial n}_{/\Gamma} + \imath \kappa u_{/\Gamma} \right) + (1 + R) f.$$

Thus, we can still have system (16) with

$$\tilde{g} = \begin{bmatrix} -\imath g \\ g \end{bmatrix} = \begin{bmatrix} -\imath R(-p+\imath q) \\ R(-p+\imath q) \end{bmatrix} + \begin{bmatrix} -\imath(1+R)f \\ (1+R)f \end{bmatrix}.$$

Let $F = \left[\begin{smallmatrix} -\imath(1+R)f \\ (1+R)f \end{smallmatrix}\right]$ and $N_R = R\left[\begin{smallmatrix} 1 & \imath \\ \imath & -1 \end{smallmatrix}\right]$. System (16) is written

$$\begin{cases} (Id+\beta)X + A_\infty^* A_\infty X - \mathbf{K}^* Y = N_R X + F - \imath\beta Y, \\ \mathbf{K}X + (\beta + A_\infty^* A_\infty)Y = \imath\beta X; \end{cases} \tag{18}$$

i.e.,

$$\mathcal{M}_\beta \begin{bmatrix} X \\ Y \end{bmatrix} = \mathcal{R}_{R,\beta} \begin{bmatrix} X \\ Y \end{bmatrix} + \begin{bmatrix} F \\ 0 \end{bmatrix}, \tag{19}$$

where

$$\mathcal{M}_\beta = \begin{bmatrix} (Id+\beta) + A_\infty^* A_\infty & -\mathbf{K}^* \\ \mathbf{K} & \beta + A_\infty^* A_\infty \end{bmatrix} \quad \text{and} \quad \mathcal{R}_{R,\beta} = \begin{bmatrix} N_R & -\imath\beta Id \\ \imath\beta Id & 0 \end{bmatrix}. \tag{20}$$

Due to the condition $|R| \leq 1$, the inf–sup condition is also satisfied, ensuring existence and unicity of the solution.

We now consider a finite element discretization of system (18). Let Γ_h be an approximation of the surface Γ, obtained by a triangulation $\mathcal{T}_h$. Let $V_h = \mathrm{Vect}\{\varphi_i;\ i = 1, N\}$, with φ_i, $i \in \{1, \ldots, N\}$ the $\mathbb{P}_1$-basis functions associated with $\mathcal{T}_h$, and with N the number of nodes of the finite element mesh Γ_h, $N \sim \kappa^2$,

$$\varphi_i \in \mathbb{P}_1, \quad \text{and} \quad \varphi_i(Nod_j) = \delta_{ij},$$

where Nod_j denotes the jth node of the finite element mesh. Let $\psi_i = \left[\begin{smallmatrix} \varphi_i \\ 0 \end{smallmatrix}\right]$ and $\psi_{i+N} = \left[\begin{smallmatrix} 0 \\ \varphi_i \end{smallmatrix}\right]$ for all i in $\{1, \ldots, N\}$. After using the variational formulation, we obtain the discrete system

$$\mathcal{M}_\beta \begin{bmatrix} X_h \\ Y_h \end{bmatrix} = \mathcal{R}_{R,\beta} \begin{bmatrix} X_h \\ Y_h \end{bmatrix} + \begin{bmatrix} F_h \\ 0 \end{bmatrix}, \tag{21}$$

where $\mathcal{M}_\beta$ and $\mathcal{R}_{R,\beta}$ are given by

$$\mathcal{M}_\beta = \begin{bmatrix} \mathcal{D}_\beta + \mathcal{A} & -\mathcal{K}^* \\ \mathcal{K} & \mathcal{B}_\beta + \mathcal{A} \end{bmatrix} \quad \text{and} \quad \mathcal{R}_{R,\beta} = \begin{bmatrix} \mathcal{N}_R & -\imath\mathcal{B}_\beta \\ \imath\mathcal{B}_\beta & 0 \end{bmatrix}, \tag{22}$$

with $\mathcal{B}_\beta, \mathcal{D}_\beta, \mathcal{K}, \mathcal{K}^*, \mathcal{A}$, and $\mathcal{N}_R$ the matrices $2N \times 2N$ and F_h the vector of size $2N$ defined by

$$\begin{aligned} (F_h)_j &= \langle F, \psi_j \rangle_{\mathbb{V}_h}, & (\mathcal{B}_\beta)_{ji} &= \langle \beta\psi_i, \psi_j \rangle_{\mathbb{V}_h}, \\ (\mathcal{D}_\beta)_{ji} &= \langle (1+\beta)\psi_i, \psi_j \rangle_{\mathbb{V}_h}, & (\mathcal{N}_R)_{ji} &= \langle N_R\psi_i, \psi_j \rangle_{\mathbb{V}_h}, \\ (\mathcal{K})_{ji} &= \langle \mathbf{K}\psi_i, \psi_j \rangle_{\mathbb{V}_h}, & (\mathcal{K}^*)_{ji} &= \langle \mathbf{K}^*\psi_i, \psi_j \rangle_{\mathbb{V}_h}, \\ (\mathcal{A})_{ji} &= \langle A_\infty\psi_i, A_\infty\psi_j \rangle_{L^2(S^2)}, \quad \text{or} & (\mathcal{A})_{ji} &= \langle \mathbf{M}\psi_i, \psi_j \rangle_{\mathbb{V}_h}, \end{aligned} \tag{23}$$

where $\mathbb{V}_h = V_h \times V_h$. The discrete inf–sup condition also confirms the existence and unicity of the solution. The finite element structure ensures that the discrete solution converges with the solution to the continuous system (19).

2.2. Solution of the Linear System

In order to solve system (21), we suggest using the relaxed Jacobi method according to the following definition. Let α be the relaxation parameter. Let $\left[\begin{smallmatrix} X_h^{(0)} \\ Y_h^{(0)} \end{smallmatrix}\right]$ be such that $Y_h^{(0)} = \imath X_h^{(0)}$. We define

$$\left(\begin{bmatrix} X_h^{(n)} \\ Y_h^{(n)} \end{bmatrix}\right)_{n\geq 1}$$

according to the relation

$$\begin{bmatrix} X_h^{(n)} \\ Y_h^{(n)} \end{bmatrix} = \alpha \begin{bmatrix} \tilde{X}_h^{(n)} \\ \tilde{Y}_h^{(n)} \end{bmatrix} + (1-\alpha) \begin{bmatrix} X_h^{(n-1)} \\ Y_h^{(n-1)} \end{bmatrix},$$

where $\left[\begin{smallmatrix} \tilde{X}_h^{(n)} \\ \tilde{Y}_h^{(n)} \end{smallmatrix}\right]$ is the solution to

$$\begin{bmatrix} \mathcal{D}_\beta + \mathcal{A} & -\mathcal{K}^* \\ \mathcal{K} & \mathcal{B}_\beta + \mathcal{A} \end{bmatrix} \begin{bmatrix} \tilde{X}_h^{(n)} \\ \tilde{Y}_h^{(n)} \end{bmatrix} = \begin{bmatrix} \mathcal{N}_R & -\imath\mathcal{B}_\beta \\ \imath\mathcal{B}_\beta & 0 \end{bmatrix} \begin{bmatrix} X_h^{(n-1)} \\ Y_h^{(n-1)} \end{bmatrix} + \begin{bmatrix} F_h \\ 0 \end{bmatrix}. \tag{24}$$

Let

$$\begin{bmatrix} V \\ W \end{bmatrix} = \begin{bmatrix} \mathcal{N}_R & -\imath\mathcal{B}_\beta \\ \imath\mathcal{B}_\beta & 0 \end{bmatrix} \begin{bmatrix} X_h^{(n-1)} \\ Y_h^{(n-1)} \end{bmatrix} + \begin{bmatrix} F_h \\ 0 \end{bmatrix}.$$

The nth iteration of the solution boils down to the solution of the following system for $\left[\begin{smallmatrix} X \\ Y \end{smallmatrix}\right]$:

$$\begin{cases} (\mathcal{D}_\beta + \mathcal{A})X - \mathcal{K}^* Y = V, \\ \mathcal{K}X + (\mathcal{B}_\beta + \mathcal{A})Y = W. \end{cases} \tag{25}$$

That is,

$$\begin{cases} X = (\mathcal{D}_\beta + \mathcal{A})^{-1}(V + \mathcal{K}^* Y), \\ \mathcal{K}(\mathcal{D}_\beta + \mathcal{A})^{-1} V + \mathcal{K}(\mathcal{D}_\beta + \mathcal{A})^{-1}\mathcal{K}^* Y + (\mathcal{B}_\beta + \mathcal{A})Y = W. \end{cases} \tag{26}$$

Thus, the point is to solve the following equation for Y:

$$(\mathcal{K}(\mathcal{D}_\beta + \mathcal{A})^{-1}\mathcal{K}^* + \mathcal{B}_\beta + \mathcal{A})Y = W - \mathcal{K}(\mathcal{D}_\beta + \mathcal{A})^{-1} V. \tag{27}$$

This solution is based on the use of the conjugate gradient method:

1. Calculation of $Z = W - \mathcal{K}(\mathcal{D}_\beta + \mathcal{A})^{-1} V$

   (i) Solution of $(\mathcal{D}_\beta + \mathcal{A})\tilde{Z} = V$ according to the conjugate gradient method with the matrix $(\mathcal{D}_\beta + \mathcal{A})$.

   (ii) $Z = W - \mathcal{K}\tilde{Z}$.

2. Solution of $(\mathcal{K}(\mathcal{D}_\beta + \mathcal{A})^{-1}\mathcal{K}^* + \mathcal{B}_\beta + \mathcal{A})Y = Z$ using a conjugate gradient method with the matrix $(\mathcal{K}(\mathcal{D}_\beta + \mathcal{A})^{-1}\mathcal{K}^* + \mathcal{B}_\beta + \mathcal{A})$. In this way, we have to perform products of the form $(\mathcal{D}_\beta + \mathcal{A})^{-1}\tilde{X}$, where $\tilde{X}$ is a given vector. This kind of product is described in 1(i).

As far as the convergence of the conjugate gradient method is concerned, we can easily check that the matrices $(\mathcal{D}_\beta + \mathcal{A})$ and $(\mathcal{K}(\mathcal{D}_\beta + \mathcal{A})^{-1}\mathcal{K}^* + \mathcal{B}_\beta + \mathcal{A})$ are Hermitian positive definite. The convergence of the relaxed Jacobi method is ensured on the assumption that $|R| < 1$. Due to the integral operators $\mathbf{K}$, $\mathbf{K}^*$, and A_∞, the calculation of the matrices $\mathcal{K}$, $\mathcal{K}^*$, and $\mathcal{A}$ implies the calculus cost $\mathcal{O}(N^2)$. Regarding $\mathcal{K}$ and $\mathcal{K}^*$, the calculation consists in performing the following expressions, $\forall i, j \in \{1, \ldots, N\}$:

$$
\begin{aligned}
&1.\quad \langle S_r\varphi_i, \varphi_j\rangle_{V_h} = \kappa \int_{\Gamma_h}\int_{\Gamma_h} G_r(x, y)\varphi_i(y)\,\overline{\varphi_j(x)}\, d\gamma(y)\, d\gamma(x),\\
&2.\quad \langle K_r\varphi_i, \varphi_j\rangle_{V_h} = \int_{\Gamma_h}\int_{\Gamma_h} \frac{\partial G_r}{\partial n_y}(x, y)\,\varphi_i(y)\overline{\varphi_j(x)}\, d\gamma(y)\, d\gamma(x),\\
&3.\quad \langle K_r'\varphi_i, \varphi_j\rangle_{V_h} = \int_{\Gamma_h}\int_{\Gamma_h} \frac{\partial G_r}{\partial n_x}(x, y)\varphi_i(y)\,\overline{\varphi_j(x)}\, d\gamma(y)\, d\gamma(x),\\
&4.\quad \langle D_r\varphi_i, \varphi_j\rangle_{V_h} = \frac{1}{\kappa}\int_{\Gamma_h}\int_{\Gamma_h} \frac{\partial^2 G_r}{\partial n_x \partial n_y}(x, y)\varphi_i(y)\overline{\varphi_j(x)}\, d\gamma(y)\, d\gamma(x).
\end{aligned}
\tag{28}
$$

The Fourth term is performed according to the formula [24]

$$
\begin{aligned}
\langle D_r\varphi_i, \varphi_j\rangle_{V_h} = \frac{1}{\kappa}\int_{\Gamma_h}\int_{\Gamma_h} G_r(x, y)[\,&\kappa^2\varphi_i(y)\,\overline{\varphi_j(x)}\,(n_x \cdot n_y)\\
&- \overrightarrow{\operatorname{curl}}_{\Gamma_h}\varphi_i(y) \cdot \overrightarrow{\operatorname{curl}}_{\Gamma_h}\overline{\varphi_j(x)}]\, d\gamma(y)\, d\gamma(x).
\end{aligned}
$$

Singularities for $x = y$ are treated according to a change of variables in the close interactions. As regards $\mathcal{A}$, the calculation is performed using the relation $(\mathcal{A})_{ji} = \langle A_\infty\psi_i, A_\infty\psi_j\rangle_{L^2(\mathcal{S}^2)}$. For the Robin case with $R = 0$, we can consider another β-system, whose solution is based on the biconjugate gradient without the relaxed Jacobi method, adding the following equations instead of (15):

$$
\begin{aligned}
-\beta X - \imath\beta Y &= 0,\\
\text{and}\quad -\imath\beta X + \beta Y &= 0.
\end{aligned}
\tag{29}
$$

Such a solution needs $\mathcal{O}(N^2)$ operations due to the matrix–vector products with the matrices $\mathcal{K}$, $\mathcal{K}^*$, and $\mathcal{A}$. The next sections deal with speeding up the solution of system (21).

3. REDUCTION OF THE SIZE OF THE SYSTEM: MICROLOCAL DISCRETIZATION

In this section, we give a short presentation of the microlocal discretization method introduced by Zhou and co-workers [1, 2, 35], assuming the following conditions are met.

- Ω is a bounded open *convex* domain in $\mathbb{R}^3$.
- u^{inc} is an incident *plane* wave.

Let $q = u_{/\Gamma}$ be the potential on the boundary Γ. Let Γ_h be a piecewise l-degree polynomial boundary. We denote by π_h the orthogonal projection from Γ_h to Γ, which is a bijection if h is small enough, where h denotes the greatest diameter of the elements of Γ_h. Consider q_h the unknown of the $\mathbb{P}_m$ finite element discrete problem based on Γ_h. We then obtain the estimates

$$\frac{\| q - \pi_h(q_h)\|_{H^s(\Gamma)}}{\|q\|_{H^s(\Gamma)}} \leq C(h\kappa)^{m+1}, \tag{30}$$

where $s = 0$ in the Dirichlet case and $s = 1/2$ in the Neumann case. These estimates involve the choice $h \sim \kappa^{-1}$. The method considered in this section permits new estimates to be obtained using an approximation of the phase function of the unknown. It stems from the coupling of finite element methods and asymptotic methods. It involves concepts of asymptotic expansions of the amplitude and the phase functions introduced by the geometrical theory of diffraction and the uniformed theory of diffraction based on ray methods (see, e.g., Bouche and Molinet [6]). The unknown writes $q = Qe^{\imath\phi}$, where Q is the amplitude and ϕ the phase function. An asymptotic behavior of the phase function is given by $\phi = \kappa\phi_0 + \mathcal{O}(\kappa^{1/3})$ [4, 21, 33]. An approximation of the phase function at the first degree is then given by $\tilde{\phi} = \kappa\phi_0$. When the obstacle is convex and the incident wave is plane, i.e., $u^{inc}(x) = e^{\imath\kappa\xi\cdot x}$, ϕ_0 is defined by $\phi_0(x) = \xi \cdot x$. Denoting by $\tilde{q}$ the new unknown such that $q = \tilde{q}e^{\imath\kappa\phi_0}$, $\tilde{q} = Qe^{\imath(\phi-\tilde{\phi})}$, new error estimates are

$$\frac{\| \tilde{q} - \pi_h(\tilde{q}_h)\|_{L^2(\Gamma)}}{\| \tilde{q} \|_{L^2(\Gamma)}} \leq C\left[h^m + h^l + \left(h\kappa^{1/3}\right)^{m+1} + \kappa h^l\right]$$

in the Dirichlet case, and

$$\frac{\| \tilde{q} - \pi_h(\tilde{q}_h)\|_{H^{1/2}(\Gamma)}}{\| \tilde{q} \|_{H^{1/2}(\Gamma)}} \leq C\left[\left(h\kappa^{1/3}\right)^{m+1} + \kappa^{3/2}h^l(\kappa h + 1)\right] \tag{31}$$

in the Neumann and Robin cases.

The error associated with the boundary approximation consists of the h^l terms. On the other hand, the h^m terms come from the finite element discretization. Thus, thanks to the term $h\kappa^{1/3}$, a new mesh can be considered with $h \sim \kappa^{-1/3}$, but due to the terms κh^l and $\kappa^{3/2}h^l(\kappa h + 1)$, we should consider a boundary approximation of degree $l \geq 3$ in the Dirichlet case and $l \geq 7$ in the Neumann and Robin cases. Such consideration is very difficult to achieve numerically. Thus, Zhou and co-workers proposed a new $\mathbb{P}_m$ finite element method based on a coarse mesh Γ_c to define the unknown and a fine mesh Γ_f to approximate the boundary Γ. h_c and h_f denote, respectively, the greatest diameter of the elements of Γ_c and Γ_f. The unknown is defined on Γ_c and the integrals are performed on the fine mesh Γ_f. New error estimates are given by the formulas

$$\frac{\| \tilde{q} - \pi_h(\tilde{q}_h)\|_{L^2(\Gamma)}}{\| \tilde{q} \|_{L^2(\Gamma)}} \leq C\left[h_c^m + h_c^{-1}h_f^{l+1} + \left(h_c\kappa^{1/3}\right)^{m+1} + \kappa h_c^{-1}h_f^{l+1}\right]$$

in the Dirichlet case, and

$$\begin{aligned}\frac{\| \tilde{q} - \pi_h(\tilde{q}_h)\|_{H^{1/2}(\Gamma)}}{\| \tilde{q} \|_{H^{1/2}(\Gamma)}} \leq C\Big[&\kappa^{1/2}h_c^{m+1/2} + \kappa^{1/2}h_f^{l+1} + \left(h_c\kappa^{1/3}\right)^{m+1} \\ &+ \left(h^l{}_f h_c^{-1}\kappa^{1/2} + \kappa^{3/2}h^l{}_f\right)(\kappa h_f + 1)\Big]\end{aligned} \tag{32}$$

in the Neumann and Robin cases .

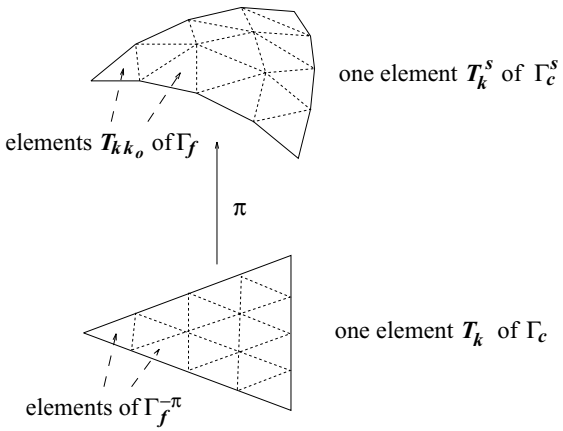

FIG. 2. Coarse mesh and fine mesh.

Γ_c is associated with the discretization of the unknown with the h_c^m terms. The h_f^l terms confirm the contribution of Γ_f to the boundary discretization. These new error estimates imply the following choices:

$$h_c \sim \kappa^{-1/3}, \quad h_f \sim \kappa^{-1}. \tag{33}$$

In the Dirichlet case, we merely need a geometric approximation with $l = 1$. In the case of both Neumann and Robin, $l \geq 3/2$ (then $l \geq 2$) is a theoretically necessary condition, but the numerical tests show that the case $l = 1$ is quite relevant.

Now, we have to introduce notations about the meshes. The unknown is defined from the coarse mesh Γ_c, with a number of nodes $N_c = \mathcal{O}(\kappa^{2/3})$. Γ_f denotes the fine mesh used to approach the surface of the obstacle, with a number of nodes $N_f = \mathcal{O}(\kappa^2)$. Actually, Γ_f will be obtained from Γ_c as follows. We first consider Γ_c a given mesh. Let $\Gamma_f^{-\pi}$ be the plane refinement of Γ_c. Then, Γ_f is obtained from $\Gamma_f^{-\pi}$ by projection onto the surface Γ of the obstacle. Due to these considerations, we subsequently denote as π the orthogonal projection from the plane triangles of Γ_c to the ones of Γ_f. π is such that $\Gamma_f = \pi(\Gamma_f^{-\pi})$. We also define Γ_c^s as the projection of Γ_c on Γ_f by π. The elements of Γ_c^s follow the surface as Γ_f does but are not plane elements (see Fig. 2).

In our case, we consider a new $\mathbb{P}_1$ finite element discretization based on Γ_c^s. The new discrete space is then defined by

$$\tilde{V}_h\big(\Gamma_c^s\big) = \big\{\tilde{q}_h / \tilde{q}_h = \tilde{q} \circ \pi^{-1}, \tilde{q}|_{T_j} \in \mathbb{P}_1(T_j)\big\},$$

where $(T_j)_j$ describes the elements of Γ_c. To simplify the notations, the subscript h denotes h_c.

Let $\psi_i = \left[\begin{smallmatrix}\varphi_i\\0\end{smallmatrix}\right]$ and $\psi_{(i+N_c)} = \left[\begin{smallmatrix}0\\\varphi_i\end{smallmatrix}\right]$ for all i in $\{1, \ldots, N_c\}$, where $\varphi_i, i \in 1, \ldots, N_c$, is the basis function associated with the ith node of the mesh Γ_c. Let $\tilde{\mathbb{V}}_h = \tilde{V}_h \times \tilde{V}_h$. The unknown is then given by $q_h = \widetilde{q_h} e^{\imath\kappa\phi_0} = \sum_{i=1}^{2N_c} \widetilde{q_i}\tilde{\psi}_i$, and $(\tilde{q}_i)_{i=1,..,2N_c}$ is the new discrete unknown, with $\tilde{\psi}_i = (\psi_i \circ \pi^{-1}) e^{\imath\kappa\phi_0}$. ψ_i is defined on Γ_c and evaluated only for points from the plane triangles of Γ_c, but the functions $\tilde{\psi}_i$ and ϕ_0 are evaluated for quadrature points of the mesh Γ_c^s.

Hence, in our case defined in the previous section, the new system has the size $\mathcal{O}(N_c \times N_c)$. Using $\tilde{\psi}_i$ like test functions, it can be written like (21),

$$\begin{bmatrix} \mathcal{D}_\beta + \mathcal{A} & -\mathcal{K}^* \\ \mathcal{K} & \mathcal{B}_\beta + \mathcal{A} \end{bmatrix} \begin{bmatrix} X_h \\ Y_h \end{bmatrix} = \begin{bmatrix} \mathcal{N}_R & -\imath\mathcal{B}_\beta \\ \imath\mathcal{B}_\beta & 0 \end{bmatrix} \begin{bmatrix} X_h \\ Y_h \end{bmatrix} + \begin{bmatrix} F_h \\ 0 \end{bmatrix}, \tag{34}$$

with the new definitions

$$\begin{aligned} (F_h)_j &= \langle F, \tilde{\psi}_j \rangle_{\tilde{\mathbb{V}}_h} = \langle F, (\psi_j \circ \pi^{-1}) e^{\imath\kappa\phi_0} \rangle_{\tilde{\mathbb{V}}_h}, \\ (\mathcal{B}_\beta)_{ji} &= \langle \beta\tilde{\psi}_i, \tilde{\psi}_j \rangle_{\tilde{\mathbb{V}}_h} = \langle \beta(\psi_i \circ \pi^{-1}) e^{\imath\kappa\phi_0}, (\psi_j \circ \pi^{-1}) e^{\imath\kappa\phi_0} \rangle_{\tilde{\mathbb{V}}_h}, \end{aligned} \tag{35}$$

and defined in the same way:

$$\begin{aligned} (\mathcal{D}_\beta)_{ji} &= \langle (1+\beta)\tilde{\psi}_i, \tilde{\psi}_j \rangle_{\tilde{\mathbb{V}}_h}, \qquad (\mathcal{N}_R)_{ji} = \langle N_R \tilde{\psi}_i, \tilde{\psi}_j \rangle_{\tilde{\mathbb{V}}_h}, \\ (\mathcal{K})_{ji} &= \langle \mathbf{K}\tilde{\psi}_i, \tilde{\psi}_j \rangle_{\tilde{\mathbb{V}}_h}, \qquad (\mathcal{K}^*)_{ji} = \langle \mathbf{K}^*\tilde{\psi}_i, \tilde{\psi}_j \rangle_{\tilde{\mathbb{V}}_h}, \\ (\mathcal{A})_{ji} &= \langle A_\infty \tilde{\psi}_i, A_\infty \tilde{\psi}_j \rangle_{L^2(\mathcal{S}^2)}. \end{aligned} \tag{36}$$

For example, the duality $\langle S_r\varphi_i, \varphi_j \rangle_{V_h}$ (28) becomes

$$\begin{aligned} \langle S_r\tilde{\varphi}_i, \tilde{\varphi}_j \rangle_{\tilde{\mathbb{V}}_h} &= \kappa \int_{\Gamma_c^s} \int_{\Gamma_c^s} G_r(x,y)\tilde{\varphi}_i(y)\overline{\tilde{\varphi}_j(x)}\, d\gamma(y)\, d\gamma(x) \\ &= \kappa \int_{\Gamma_f} \int_{\Gamma_f} G_r(x,y)\tilde{\varphi}_i(y)\overline{\tilde{\varphi}_j(x)}\, d\gamma(y)\, d\gamma(x) \\ &= \kappa \sum_{k/T_k^s \cap \operatorname{supp}(\varphi_i) \neq \emptyset} \sum_{k_0} \sum_{l/T_l^s \cap \operatorname{supp}(\varphi_j) \neq \emptyset} \sum_{l_0} \int_{T_{kk_0}} \int_{T_{ll_0}} G_r(x,y) \\ &\quad \times \varphi_i(\pi^{-1}(y)) e^{\imath\kappa\phi_0(y)} \overline{\varphi_j(\pi^{-1}(x)) e^{\imath\kappa\phi_0(x)}}\, d\gamma(y)\, d\gamma(x), \end{aligned} \tag{37}$$

where we denote by $\{T_{kk_0}\}_{k_0}$ the set of triangles of Γ_f that make up T_k^s (see Fig. 2).

The new system (34) has the same properties as the previous one (21) due to the particular choice of the test functions. Thus, we select the same resolution, given in Section 2.2.

Hence, we obtain a problem whose size is $\mathcal{O}(\kappa^{4/3})$ instead of $\mathcal{O}(\kappa^4)$. Thus, the memory cost is much less, but due to the performing of the matrices with respect to the consideration of the fine mesh Γ_f, the matrices calculation still requires $\mathcal{O}(\kappa^4)$ operations. To reduce the cost, the authors Zhou and co-workers suggested using the theory of the stationary phase [19]. However, the numerical approach of this theory is very complicated and implies difficulties not yet solved in 3-D. In the next section we present a study of the FMM in order to speed up the calculation of the matrices (see Section 5) without the theory of the stationary phase.

4. ACCELERATION OF THE CALCULATION: THE ONE-LEVEL FAST MULTIPOLE METHOD

The fast multipole method is a robust method that speeds up the calculation of the matrix–vector products of the iterative solution. We briefly present the one-level fast multipole method. For further information, we refer the reader to recent articles written by Darve [11–13] for the multilevel FMM and to previous articles [8, 28].

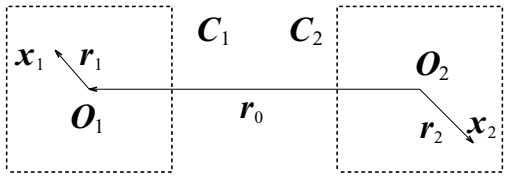

FIG. 3. Interaction between x_1 and x_2.

The method is based on two developments. Through groups of elements, an uncoupling between two points is established using the Gegenbauer series and an integral around the unit sphere S^2. The obstacle is included inside a cube. Subdividing recursively the cube as an oct-tree, we obtain the groups of elements considering the boxes of the finest level. Let $x_1, x_2 \in \Gamma_h$. Let O_1, O_2 be the centers of the two boxes C_1 and C_2, including x_1 and x_2 (Fig. 3). Then, $x_1 - x_2 = r_0 + r$, where $r_0 = O_1 - O_2$, $r = r_1 - r_2$, and $r_i = x_i - O_i$. With $|r_0| > |r|$ the expansion of the Green function used by the multipole method is given by the formula (see [3])

$$\frac{e^{\imath\kappa|x_1-x_2|}}{4\pi|x_1-x_2|} \approx \frac{\imath\kappa}{(4\pi)^2}\sum_{p=1}^{P}\omega_p e^{\imath\kappa\langle s_p,r_1\rangle}T_{L,r_0}(s_p)e^{-\imath\kappa\langle s_p,r_2\rangle}, \tag{38}$$

with

$$T_{L,r_0}(s) = \sum_{m=0}^{L}(2m+1)\imath^m h_m^{(1)}(\kappa|r_0|)P_m(\cos(s,r_0)).$$

The integer L is the truncation parameter of the Gegenbauer series and P the number of discrete directions $\{s_p,\ p = 1,\ldots,P\}$ corresponding to a numerical quadrature on the unit sphere S^2. The quadrature generally considered consists of a trapezoidal quadrature in the φ direction and a Gauss–Legendre quadrature in the $\cos\theta$ direction, where (ρ,θ,φ) is the spherical coordinate system [12, 20, 25]. Recent studies of Chew and co-workers [20] validate, for relatively large values of κd, the empirical formula

$$L = \kappa d + C(\kappa d)^{1/3}, \tag{39}$$

where d is the diameter of the multipole boxes and C depends only on the desired accuracy. Next, P is given as

$$P = (L+1)(2L+1). \tag{40}$$

We suggest the application of the one-level FMM to speed up the matrix–vector products whose matrix is, respectively, $\mathcal{K}$, $\mathcal{K}^*$, and $\mathcal{A}$, defined for the IE system in Section 2. New integral kernels and developments are considered here (see [22]). For the singular integral kernel of the IE system, where the matrix is $\mathcal{K}$ or $\mathcal{K}^*$ (see [3, p. 440]), we have the multipole approximation

$$\begin{aligned}\frac{\cos(\kappa|x_1-x_2|)}{4\pi|x_1-x_2|} &\approx \frac{-\kappa}{(4\pi)^2}\sum_{p=1}^{P}\omega_p e^{\imath\kappa\langle s_p,r_1\rangle}T^{\Re}_{L,r_0}(s_p)e^{-\imath\kappa\langle s_p,r_2\rangle},\\ \text{with}\quad T^{\Re}_{L,r_0}(s) &= \sum_{m=0}^{L}(2m+1)\imath^m y_m(\kappa|r_0|)P_m(\cos(s,r_0)).\end{aligned} \tag{41}$$

The normal derivative of the integral kernel has the following approximation, where $j = 1, 2$:

$$\partial_{n_j} \frac{\cos(\kappa|x_1 - x_2|)}{4\pi|x_1 - x_2|} \approx \frac{(-1)^j \imath \kappa^2}{(4\pi)^2} \sum_{p=1}^{P} \omega_p \langle s_p, n(x_j)\rangle e^{\imath\kappa\langle s_p, r_1\rangle} T^{\Re}_{L,r_0}(s_p) e^{-\imath\kappa\langle s_p, r_2\rangle}. \quad (42)$$

After derivation, P must be slightly greater than it was, as Rahola showed [25]. As well as for the classical case, the previous approximations are available for far interactions (condition $|r_0| > |r|$).

We now study the case of the matrix $\mathcal{A}$, with the regular integral kernel of the IE system. We then consider the relation $(\mathcal{A})_{ji} = \langle \mathbf{M}\psi_i, \psi_j\rangle_{\mathbb{V}_h}$. Due to the regularity of the integral kernel, the approximation can be written for all x_1, x_2. Thus, the far and close interactions are approximated in the same way,

$$\begin{aligned} &\frac{\sin(\kappa|x_1 - x_2|)}{4\pi|x_1 - x_2|} \approx \frac{\kappa}{(4\pi)^2} \sum_{p=1}^{P} \omega_p e^{\imath\kappa\langle s_p, r_1\rangle} T^{\Im}_{L,r_0}(s_p) e^{-\imath\kappa\langle s_p, r_2\rangle} \\ &\text{with} \quad T^{\Im}_{L,r_0}(s) = \sum_{m=0}^{L} (2m+1)\imath^m j_m(\kappa|r_0|) P_m(\cos(s, r_0)). \end{aligned} \quad (43)$$

The normal derivative of the integral kernel has the following approximation, for $j = 1, 2$:

$$\partial_{n_j} \frac{\sin(\kappa|x_1 - x_2|)}{4\pi|x_1 - x_2|} \approx \frac{(-1)^{j+1} \imath \kappa^2}{(4\pi)^2} \sum_{p=1}^{P} \omega_p \langle s_p, n(x_j)\rangle e^{\imath\kappa\langle s_p, r_1\rangle} T^{\Im}_{L,r_0}(s_p) e^{-\imath\kappa\langle s_p, r_2\rangle}, \quad (44)$$

$$\partial_{n_1}\partial_{n_2} \frac{\sin(\kappa|x_1 - x_2|)}{4\pi|x_1 - x_2|} \approx \frac{\kappa^3}{(4\pi)^2} \sum_{p=1}^{P} \omega_p \langle s_p, n(x_1)\rangle \langle s_p, n(x_2)\rangle e^{\imath\kappa\langle s_p, r_1\rangle} T^{\Im}_{L,r_0}(s_p) e^{-\imath\kappa\langle s_p, r_2\rangle}. \quad (45)$$

We give, for example, the algorithm of the fast product $\mathcal{M}\,Y$ for a given vector Y and with the matrix $\mathcal{M}$ defined by

$$\forall i, j \in \{1, \ldots, N\}, \quad \mathcal{M}_{ij} = \overline{\alpha_i}\alpha_j G_r(x_i, x_j), \quad \alpha_i, \alpha_j \in \mathbb{C}.$$

The matrix stands for a discretization of (28.1). We apply the one-level FMM using relation (41). Let N_{fmm} be the number of FMM boxes. Due to the condition $|r_0| > |r|$, we consider the close part and the far part of the matrix, for x_i in a FMM box C and x_j in a FMM box $\tilde{C}$,

$$(\mathcal{M}^{far})_{ij} = \begin{cases} 0 & \text{if } \tilde{C} \text{ close to } C, \\ \mathcal{M}_{ij} & \text{if } \tilde{C} \text{ far from } C, \end{cases} \quad (\mathcal{M}^{close})_{ij} = \begin{cases} \mathcal{M}_{ij} & \text{if } \tilde{C} \text{ close to } C, \\ 0 & \text{if } \tilde{C} \text{ far from } C, \end{cases} \quad (46)$$

where "$\tilde{C}$ close to C" means that the cubes $\tilde{C}$ and C have at least one common vertex. The multipole approximation is given by the following relation, for all i in $\{1, \ldots, N\}$, x_i in a box C:

$$(\mathcal{M}^{far}\,Y)_i \approx \Psi_i \equiv \frac{-\kappa}{(4\pi)^2} \overline{\alpha_i} \sum_{p=1}^{P} \omega_p e^{\imath\kappa\langle s_p, r_i\rangle} \sum_{\tilde{C} \text{ far from } C} T^{\Re}_{L,r_{C\tilde{C}}}(s_p) \sum_{j/x_j \in \tilde{C}} e^{-\imath\kappa\langle s_p, r_j\rangle} \alpha_j Y_j. \quad (47)$$

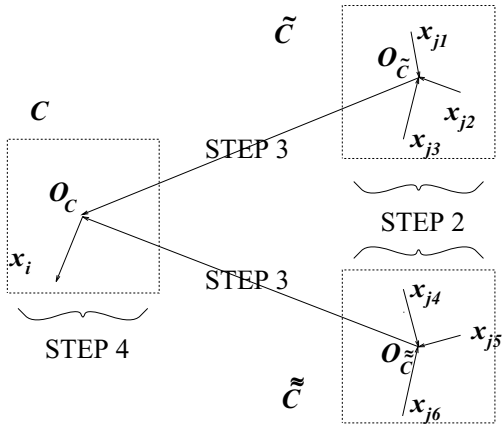

FIG. 4. Far interactions.

Thus, the algorithm of the calculation of the matrix–vector product $\mathcal{M}^{far}Y$, using the one-level FMM, consists of four steps (Fig. 4).

Step 1. Tansfer functions: Translation between two boxes $T^{\Re}_{L,O_C-O_{\tilde{C}}}(s_p)$ defined in (41), $\forall(O_C - O_{\tilde{C}})$, with C and $\tilde{C}$ two far FMM boxes, $\forall p \in \{1, \ldots, P\}$.

Step 2. Radiation functions: $\forall \tilde{C}$ FMM box, $\forall p \in \{1, \ldots, P\}$,

$$F_{\tilde{C}}(s_p) = \sum_{j/x_j \in \tilde{C}} e^{\imath\kappa\langle s_p, O_{\tilde{C}} - x_j\rangle}\alpha_j Y_j.$$

Step 3. Transfer from $\tilde{C}$ to C: $\forall C$ FMM box, $\forall p \in \{1, \ldots, P\}$,

$$G_C(s_p) = \sum_{\tilde{C} \text{ far from } C} T^{\Re}_{L,O_C-O_{\tilde{C}}}(s_p) F_{\tilde{C}}(s_p).$$

Step 4. Integration on S^2: $\forall i \in \{1, \ldots, N\}$, $x_i \in C$ FMM box,

$$\Psi_i = \frac{-\kappa}{(4\pi)^2}\overline{\alpha_i}\sum_{p=1}^{P} \omega_p e^{\imath\kappa\langle s_p, x_i - O_C\rangle} G_C(s_p).$$

The other discrete calculations of the products with the matrices $\mathcal{K}$ and $\mathcal{K}^*$ are performed in the same way, using relations (41) and (42). We mean also to calculate products with $\mathcal{A}$ in the same way, using relations (43)–(45). Moreover, this matrix enables us to perform close interactions as well as far ones.

Choosing a number of FMM boxes $N_{fmm} \sim N^{1/2}$, we obtain an algorithm with the complexity $\mathcal{O}(N^{3/2})$, i.e., $\mathcal{O}(\kappa^3)$ [8].

5. COUPLING: MICROLOCAL DISCRETIZATION AND FAST MULTIPOLE METHOD

The coupling is based on the reduction of the size of the system using the approximation of the phase function, and on the acceleration of the matrix calculation using the one-level FMM. The one-level FMM is considered instead of the theory of the stationary phase. The matrix–vector product is then performed in a classical way. Due to the approximation of the phase function, we have to consider the coarse mesh (introduced in Section 3). The unknown is defined on the coarse mesh and, in order to have a good geometrical approximation of Γ, we resort to the fine mesh which is used in classical methods. For the multipole method, the elements of the fine mesh are grouped in boxes (Fig. 5). Then, we consider the approximation of the phase function given by the microlocal discretization. Using the notations listed in Section 3, we consider the same system (34)–(36),

$$\begin{bmatrix} \mathcal{D}_\beta + \mathcal{A} & -\mathcal{K}^* \\ \mathcal{K} & \mathcal{B}_\beta + \mathcal{A} \end{bmatrix} \begin{bmatrix} X_h \\ Y_h \end{bmatrix} = \begin{bmatrix} \mathcal{N}_R & -\imath\mathcal{B}_\beta \\ \imath\mathcal{B}_\beta & 0 \end{bmatrix} \begin{bmatrix} X_h \\ Y_h \end{bmatrix} + \begin{bmatrix} F_h \\ 0 \end{bmatrix}, \tag{48}$$

with the definitions

$$(F_h)_j = \langle F, \tilde{\psi}_j \rangle_{\tilde{\mathbb{V}}_h} = \langle F, (\psi_j \circ \pi^{-1}) e^{\imath\kappa\phi_0} \rangle_{\tilde{\mathbb{V}}_h}, \tag{49}$$

$$(\mathcal{B}_\beta)_{ji} = \langle \beta\tilde{\psi}_i, \tilde{\psi}_j \rangle_{\tilde{\mathbb{V}}_h} = \langle \beta(\psi_i \circ \pi^{-1}) e^{\imath\kappa\phi_0}, (\psi_j \circ \pi^{-1}) e^{\imath\kappa\phi_0} \rangle_{\tilde{\mathbb{V}}_h}, \tag{50}$$

in the same way:

$$(\mathcal{D}_\beta)_{ji} = \langle (1+\beta)\tilde{\psi}_i, \tilde{\psi}_j \rangle_{\tilde{\mathbb{V}}_h}, \quad (\mathcal{N}_R)_{ji} = \langle N_R \tilde{\psi}_i, \tilde{\psi}_j \rangle_{\tilde{\mathbb{V}}_h}, \tag{51}$$

$$(\mathcal{K})_{ji} = \langle \mathbf{K}\tilde{\psi}_i, \tilde{\psi}_j \rangle_{\tilde{\mathbb{V}}_h}, \quad (\mathcal{K}^*)_{ji} = \langle \mathbf{K}^*\tilde{\psi}_i, \tilde{\psi}_j \rangle_{\tilde{\mathbb{V}}_h}, \tag{52}$$

$$(\mathcal{A})_{ji} = \langle \mathbf{M}\tilde{\psi}_i, \tilde{\psi}_j \rangle_{\tilde{\mathbb{V}}_h}. \tag{53}$$

The matrices $\mathcal{B}_\beta$, $\mathcal{D}_\beta$, and $\mathcal{N}_R$ are performed in a classical way with $\mathcal{O}(N_f)$ operations. In order to speed up the calculation of the matrices $\mathcal{K}$, $\mathcal{K}^*$, and $\mathcal{A}$, we use the one-level FMM instead of the stationary phase, as described below. We recall that $\{T_{k\,k_0}\}_{k_0}$ is the set of triangles of Γ_f that make up T_k^s. Let us consider the matrix $\mathcal{M}$ defined as follows, $\forall i, j \in \{1, \ldots, N_c\}$,

$$\mathcal{M}_{ij} = \sum_{k/T_k^s \cap \operatorname{supp}(\varphi_i) \neq \varnothing} \; \sum_{l/T_l^s \cap \operatorname{supp}(\varphi_j) \neq \varnothing} \; \sum_{T_{kk_0}} \sum_{T_{ll_0}} \overline{\alpha_{kk_0} e^{\imath\kappa\phi_0(x_{kk_0})}}\, \alpha_{ll_0} e^{\imath\kappa\phi_0(x_{ll_0})} G_r\left(x_{kk_0}, x_{ll_0}\right),$$

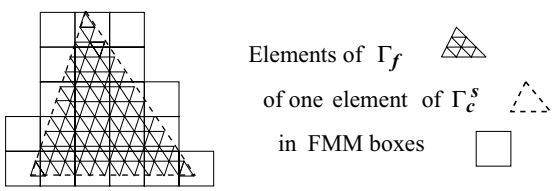

FIG. 5. Meshes and FMM boxes.

with $\alpha_{kk_0}, \alpha_{ll_0} \in \mathbb{C}$. The matrix stands for a discretization of (28.1) with our new definitions (52). We apply the one-level FMM separating the close part from the far part of the matrix and using relation (41). Thus, the multipole approximation is given for all i, j in $\{1, \ldots, N_c\}$ by

$$\left(\mathcal{M}^{far}_{approx}\right)_{ij} = \frac{-\kappa}{(4\pi)^2} \sum_{p=1}^{P} \omega_p \sum_{k/T_k^s \cap \operatorname{supp}(\varphi_i) \neq \emptyset} \sum_{C/T_k^s \cap C \neq \emptyset} \sum_{k_0/x_{kk_0} \in C} \overline{\alpha_{kk_0}} \overline{e^{\imath \kappa \phi_0(x_{kk_0})}} e^{\imath \kappa \langle s_p, r_{kk_0} \rangle}$$
$$\times \sum_{l/T_l^s \cap \operatorname{supp}(\varphi_j) \neq \emptyset} \sum_{\substack{\tilde{C}/T_l^s \cap \tilde{C} \neq \emptyset \\ \tilde{C} \text{ far from } C}} T^{\Re}_{L, r_{C\tilde{C}}}(s_p) \sum_{l_0/x_{ll_0} \in \tilde{C}} \alpha_{ll_0} e^{\imath \kappa \phi_0(x_{ll_0})} e^{-\imath \kappa \langle s_p, r_{ll_0} \rangle}, \quad (54)$$

with L and P defined by (39) and (40). Hence, the algorithm of the calculation of the matrix $\mathcal{M}^{far}$, using the one-level FMM, consists of three steps.

Step 1. Tansfer functions: $\forall (O_C - O_{\tilde{C}})$, $\tilde{C}$ far from C, $\forall p \in \{1, \ldots, P\}$,

$$T^{\Re}_{L, O_C - O_{\tilde{C}}}(s_p) = \sum_{m=0}^{L} (2m+1) \imath^m y_m(\kappa |O_C - O_{\tilde{C}}|) P_m(\cos(s_p, O_C - O_{\tilde{C}})).$$

Step 2. New radiation functions: $\forall i \in \{1, \ldots, N_c\}$, $\forall k / T_k^s \cap \operatorname{supp}(\varphi_i) \neq \emptyset$, $\forall C$ FMM box such that $T_k^s \cap C \neq \emptyset$, $\forall p \in \{1, \ldots, P\}$,

$$F_{kC}(s_p) = \sum_{k_0/x_{kk_0} \in C} \alpha_{kk_0} e^{\imath \kappa \phi_0(x_{kk_0})} e^{\imath \kappa \langle s_p, O_C - x_{kk_0} \rangle}.$$

Step 3. Approximation of the matrix, $\forall i, j \in \{1, \ldots, N_c\}$,

$$\left(\mathcal{M}^{far}_{approx}\right)_{ij} = \frac{-\kappa}{(4\pi)^2} \sum_{p=1}^{P} \omega_p \sum_{k/T_k^s \cap \operatorname{supp}(\varphi_i) \neq \emptyset} \sum_{C/T_k^s \cap C \neq \emptyset} \overline{F_{kC}(s_p)}$$
$$\times \sum_{l/T_l^s \cap \operatorname{supp}(\varphi_j) \neq \emptyset} \sum_{\substack{\tilde{C}/T_l^s \cap \tilde{C} \neq \emptyset \\ \tilde{C} \text{ far from } C}} T^{\Re}_{L, O_C - O_{\tilde{C}}}(s_p) F_{l\tilde{C}}(s_p).$$

Then, a matrix–vector product with the matrix $\mathcal{M}$ is approximated by the following calculation, $\forall i \in \{1, \ldots, N_c\}$,

$$(\mathcal{M}\, Y)_i = \sum_{j=1}^{N_c} \left((\mathcal{M}^{close})_{ij} + \left(\mathcal{M}^{far}_{approx}\right)_{ij} \right) Y_j,$$

where $\mathcal{M}^{close}$ is performed in a classical way.

The other discrete calculations of the matrices $\mathcal{K}$ and $\mathcal{K}^*$ are performed in the same way, using relations (41) and (42). The relations (43)–(45) enable one to perform a multipole approximation of the matrix $\mathcal{A}$. Denoting by N_{fmm} the number of FMM boxes, the new theoretical complexity of the calculation cost is given for a product $\mathcal{M}\, Y$ in Table I, where $\mathcal{M}$ is one of the matrices $\mathcal{K}$, $\mathcal{K}^*$, and $\mathcal{A}$. The memory cost has the complexity $\mathcal{O}(\max(N_{fmm}, N_c) \frac{N_f}{N_{fmm}} + N_c^2)$.

TABLE I
Calculation Cost

	Independent of Y	Dependent on Y
$\mathcal{M}^{far}$	$\sim 8LN_f + \dfrac{N_f^2}{N_{fmm}} + \max\left(N_{fmm}^2, N_c^2\right)\dfrac{N_f}{N_{fmm}}$	$\sim N_c^2$
$\mathcal{M}^{close}$	$\sim \dfrac{N_f^2}{N_{fmm}}$	$\sim N_c^2$

Concerning the number of FMM boxes, the optimal choice is then $N_{fmm} \sim N_f^{1/2}$. Thus, the number of FMM boxes, N_{fmm} is greater than N_c. Now, we can compare the different methods (Table II).

With our new method, the calculation which is independent of Y corresponds to the matrix calculation and is performed once. On the other hand, the calculation that is dependent on Y is performed to each iteration. Let N_{iter} be the number of iterations within the iterative solution of the system. The global CPU time of our new method is then $\mathcal{O}(N_f^{3/2} + N_{iter}\, N_f^{2/3})$. With the one-level FMM, users classically store the part of the matrix corresponding to the close iteractions that are performed once. That implies the complexity given between brackets. However, in order to consider industrial test cases, we do not store the close part of the matrix and we perform them to each iteration. Hence, our one-level FMM has a CPU time of complexity $\mathcal{O}(N_f^{5/4} + N_{iter}\, N_f^{3/2})$ and requires a storage of complexity $\mathcal{O}(N_f)$. Anyway, our method appears more efficient than the one-level FMM for all N_{iter}. Moreover, due to the difficulties of the theory of the stationary phase in 3-D, our new method is more robust than the microlocal discretization with stationary phase and obviously more efficient than the microlocal discretization without stationary phase.

6. NUMERICAL RESULTS

In order to validate the new method, four codes were written. The first one denoted by $\mathcal{C}$(IE) solves the IE system in a classical way, as defined in Section 2. The second code, $\mathcal{C}$(IE + FMM), is a variant of the previous one, speeding up the matrix–vector products using the one-level FMM, as explained in Section 4. The third one, $\mathcal{C}$(IE + MD), is an application of the microlocal discretization method to the IE system, as explained in Section 3. The code $\mathcal{C}$(IE + MD + FMM) is an application of the coupling of both microlocal discretization and one-level FMM to the IE system, which we described in Section 5. As regards the IE system, the parameter β of the β-system (16) is chosen equal to 0.5. The relaxation parameter of

TABLE II
Comparison of Methods

Method	Calculation independent of Y	Calculation dependent on Y	Memory
Microlocal discretization without stationary phase	$\sim N_f^2$	$\sim N_f^{2/3}$	$\sim N_f$
One-level FMM $\left(N_{fmm} \sim N_f^{1/2}\right)$	$\sim N_f^{5/4}$ $\left(\text{or } N_f^{3/2}\right)$	$\sim N_f^{3/2}$	$\sim N_f$ $\left(\text{or } N_f^{3/2}\right)$
New method $\left(N_{fmm} \sim N_f^{1/2}\right)$	$\sim N_f^{3/2}$	$\sim N_f^{2/3}$	$\sim N_f$

the relaxed Jacobi method is set equal to 0.7 (see Section 2.2). Concerning the FMM, the number of terms in the Gegenbauer series is defined by $L = \kappa d + C(\kappa d)^{1/3}$, where d is the diameter of the multipole boxes, with $C = 6$ (see Section 4). In addition, we denote by JM the Jacobi method, GC1 the conjugate gradient applied to the matrix $(\mathcal{D}_\beta + \mathcal{A})$ (see Section 2.2), and GC2 the second conjugate gradient. In this section, we also denote by N_f, N_c, and N_{fmm}, the number of triangles of Γ_f, the number of triangles of Γ_c, and the number of FMM boxes. The fine mesh Γ_f has an average edge length of about $\lambda/10$ for the sphere and about $\lambda/7$ for the Cetaf, the industrial test case. All the results are obtained on a EV67 processor of a Compaq cluster ES40.

We first present numerical tests for a sphere with a diameter $D = 2$ m, which allows us to compare numerical solutions with the exact solution, the Mie series solution. Comparisons are made considering the bistatic RCS (radar cross section). The results are obtained with the residual 10^{-4} and 10^{-3}, respectively, for GC1 and GC2, and the relative difference 10^{-3} between two iterates of JM. With the sphere, we consider a plane incident wave of direction $(0, 0, -1)$. Figure 6 validates $\mathcal{C}(\mathrm{IE})$ and the FMM contribution in $\mathcal{C}(\mathrm{IE} + \mathrm{FMM})$. Regarding CPU time and memory requirements, we can give the gain which results from the FMM approximation. The difference for the CPU time derives from the nonuse of the Jacobi relaxed method for the Robin case $R = 0$ (see Section 2.2). Concerning accuracy,

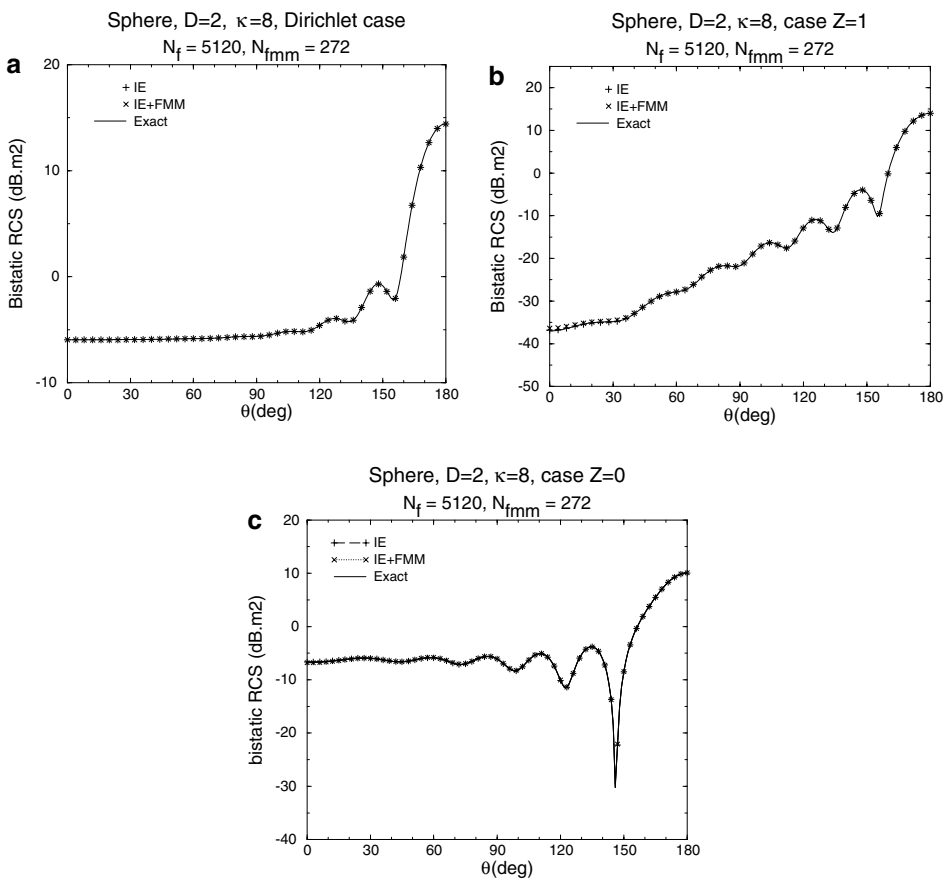

FIG. 6. $\mathcal{C}(\mathrm{IE})$–$\mathcal{C}(\mathrm{IE} + \mathrm{FMM})$, for $\kappa = 8$. (a) Dirichlet case; (b) Robin case; (c) Neumann case.

TABLE III
$\mathcal{C}$(IE) and $\mathcal{C}$(IE + FMM): Cost and Accuracy

Figure		CPU time (s)	Memory	$Y_\iota X$	Err(AD)
6a	$\mathcal{C}$(IE)	15,256	682 MB	2.3×10^{-3}	0.6×10^{-4}
	$\mathcal{C}$(IE + FMM)	6,048	522 MB	9.1×10^{-3}	1.3×10^{-4}
6b	$\mathcal{C}$(IE)	11,311	682 MB	3.8×10^{-3}	0.4×10^{-3}
	$\mathcal{C}$(IE + FMM)	546	521 MB	8.9×10^{-3}	1.5×10^{-3}
6c	$\mathcal{C}$(IE)	17,701	682 MB	3.1×10^{-3}	0.5×10^{-3}
	$\mathcal{C}$(IE + FMM)	8,450	522 MB	9.4×10^{-3}	0.6×10^{-3}

Table III shows the good behavior of the FMM. Err(AD) denotes the relative error in l^2-average made on the diffusion amplitude in comparison with the Mie series solution and $Y_\iota X$ denotes the relative error $\frac{\|Y_h - \iota X_h\|_2}{\|X_h\|_2}$ which converges to 0. Actually, relation (17) leads to good criteria of accuracy; such criteria does not exist for other integral formulations [31]. For small test cases, Fig. 7 shows that the coupling $\mathcal{C}$(IE + MD + FMM) enables one to obtain results similar to the microlocal discretization method $\mathcal{C}$(IE + MD) but with a CPU time clearly less than that of $\mathcal{C}$(IE + MD). Thus, for large test cases, we only validate the coupling $\mathcal{C}$(IE + MD + FMM). We can also give the gain which results from the FMM approximation and the accuracy of the different tests in Table IV. The costs with $\mathcal{C}$(IE), given in Table III, are recalled for comparison.

We now validate the code $\mathcal{C}$(IE + MD + FMM) by considering higher frequencies with the sphere. Figures 8 and 9 show excellent results obtained for the Dirichlet boundary condition. The numerical error is given in Table V. Figure 10 shows the results regarding CPU time and memory requirements with log–log curves. Concerning the one-level FMM, it was used with rather small cases. Thus, these results are not significant for the one-level FMM.

Figure 10 shows that our new method is very efficient. Considering a fine mesh with an average edge length of about $\lambda/10$, we can choose a coarse mesh with an average edge length of about λ/C_κ, where C_κ decreases when κ increases. The case illustrated in Fig. 9

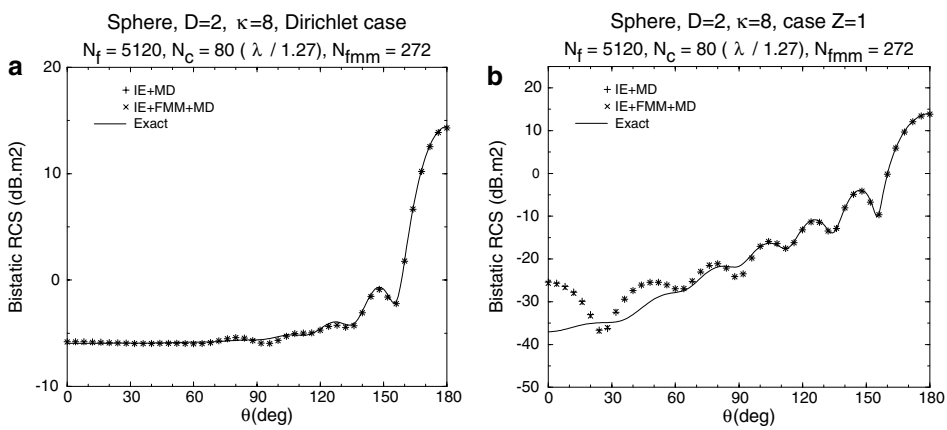

FIG. 7. $\mathcal{C}$(IE + MD)–$\mathcal{C}$(IE + MD + FMM), for $\kappa = 8$. (a) Dirichlet case; (b) Robin case.

TABLE IV
$\mathcal{C}$(IE + MD) and $\mathcal{C}$(IE + MD + FMM): Cost and Accuracy

Figure		CPU time (s)	Memory	$Y \imath X$	Err(AD)
7a	$\mathcal{C}$(IE)	15,256	682 MB	2.3×10^{-3}	0.6×10^{-4}
	$\mathcal{C}$(IE + MD)	1,613	12 MB	1.2×10^{-2}	1.5×10^{-3}
	$\mathcal{C}$(IE + MD + FMM)	183	37 MB	1.3×10^{-2}	1.5×10^{-3}
7b	$\mathcal{C}$(IE)	11,311	682 MB	3.8×10^{-3}	0.4×10^{-3}
	$\mathcal{C}$(IE + MD)	1,599	12 MB	2.5×10^{-2}	5.3×10^{-2}
	$\mathcal{C}$(IE + MD + FMM)	181	37 MB	2.6×10^{-2}	5.1×10^{-2}

TABLE V
Accuracy with the Dirichlet Boundary Condition

Figure	κ	N_f	N_c	$Y \imath X$	Err(AD)
8a	12	11,520	180	6.6×10^{-3}	1.2×10^{-3}
8b	24	46,080	720	3×10^{-3}	1×10^{-3}
9	84	327,680	1280	1.7×10^{-3}	0.9×10^{-3}

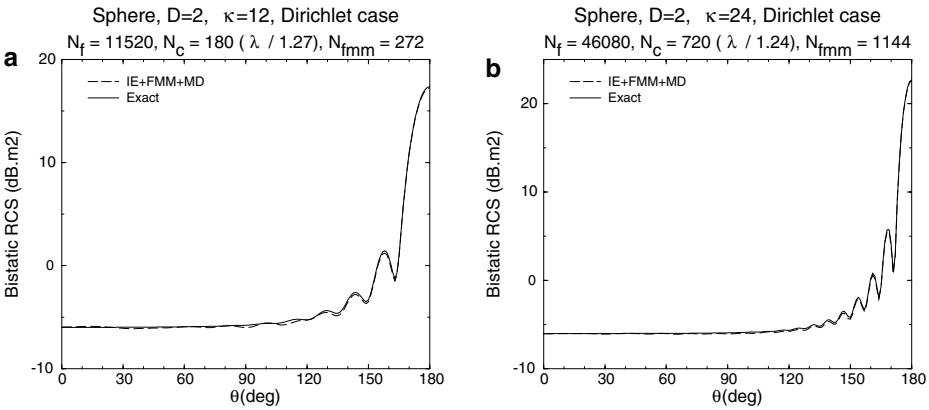

FIG. 8. $\mathcal{C}$(IE + MD + FMM), Dirichlet case. (a) $\kappa = 12$; (b) $\kappa = 24$.

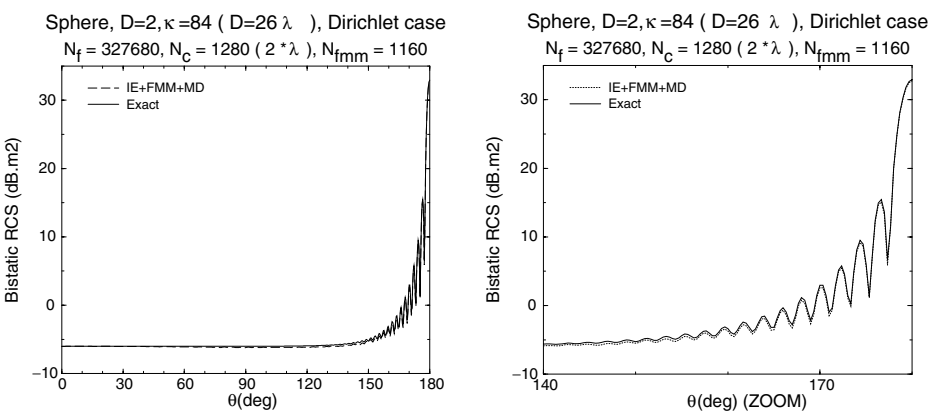

FIG. 9. $\mathcal{C}$(IE + MD + FMM), Dirichlet case, $D = 26\lambda$.

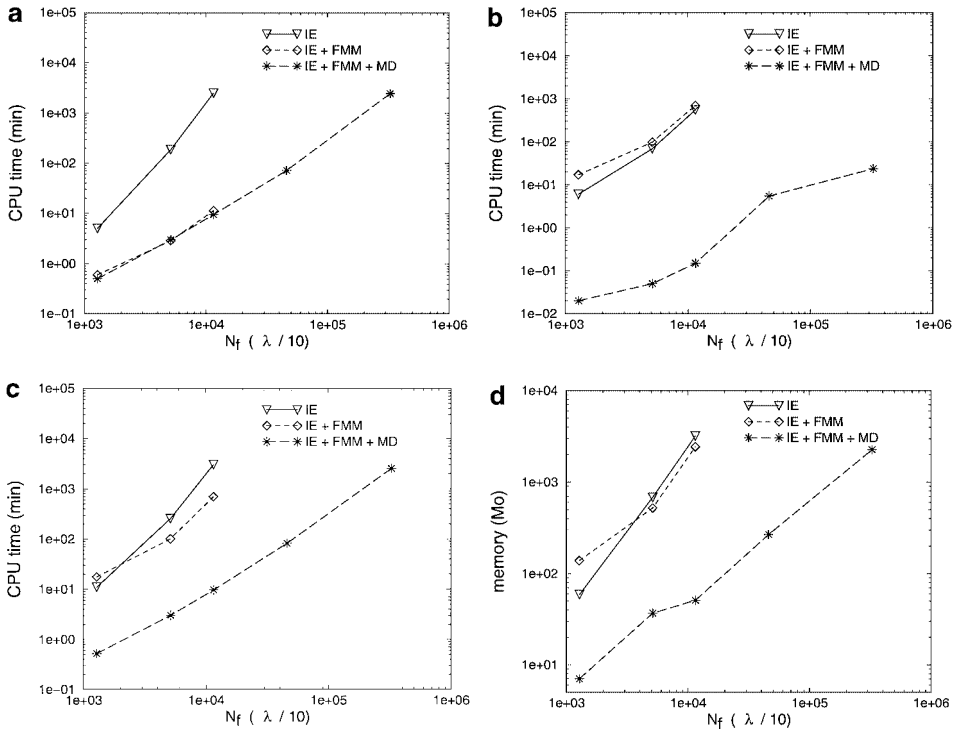

FIG. 10. CPU time and memory requirements. (a) Precalculation; (b) resolution; (c) total CPU time; (d) memory requirements.

is interesting with a coarse mesh where $C_\kappa = 0.5$, i.e., an average edge length of about 2λ. The frequencies considered are not large enough to validate the behavior $N_c \sim {N_f}^{1/3}$ estimated by the theory. However, we can plot a first curve concerning N_c as a function of N_f (see Fig. 11).

We can already see that the behavior of N_c as a function of N_f, or as a function of the frequency, is promising. We give now information about the numbers of iterations in the

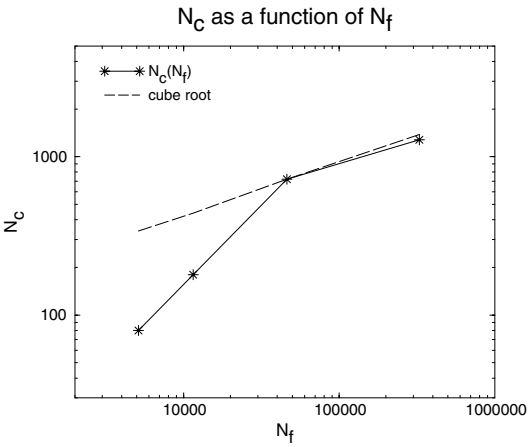

FIG. 11. $N_c(N_f)$.

TABLE VI
Numbers of Iterations

κ	8	12	24	84
IE	$11-8-19$	$10-8-20$		
IE + FMM + MD	$10-9-16$	$11-9-15$	$12-10-13$	$13-12-12$

iterative resolution. In Table VI, the numbers of iterations are given in the form $a-b-c$, which are the numbers of iterations respectively of GC1, GC2, and JM. The numbers of iterations do not increase with κ and the new method does not damage the convergence of the iterative methods. Moreover, for the code $\mathcal{C}$(IE + MD + FMM), when the wavenumber increases, the number of iterations of JM decreases, as does the error on $\| Y_h - \imath X_h \|_2$, given in Table V.

Although results do not prove to be as good in both Neumann and Robin cases, probably because the approximation of the surface is of degree $l = 1$ (see error estimations), they are still quite relevant. Figures 12 and 13 give results for the Neumann boundary condition and the Robin boundary condition with the impedance $Z = 1$. As regards memory requirements and CPU time, both Neumann and Robin cases are similar to the Dirichlet one. For the Neumann case, the accuracy is given in Table VII. For the Robin case, results are given in Fig. 13 and the accuracy is given in Table VIII.

In this section, we have presented results such that the coarse mesh has an average edge length of about λ/C_κ, with C_κ becoming smaller and smaller for the same accuracy when κ increases. Thus, the memory requirements and resolution time are less than those of the other methods. Nevertheless, the matrix calculation deserves acceleration. We are hopeful that CPU time will be further reduced using a multilevel FMM instead of the one-level FMM.

Concerning the Cetaf, due to a concavity, the condition of convexity is not met. The results are not as good as the ones obtained for the sphere; however they are also quite interesting, as explained below. The results are given below with the incident plane wave of direction $(0, -\sqrt{2}/2, -\sqrt{2}/2)$, which hits the Cetaf at an angle of 45°. We used a fine mesh with an average edge length of about $\lambda/7$ and a coarse mesh with an average edge length

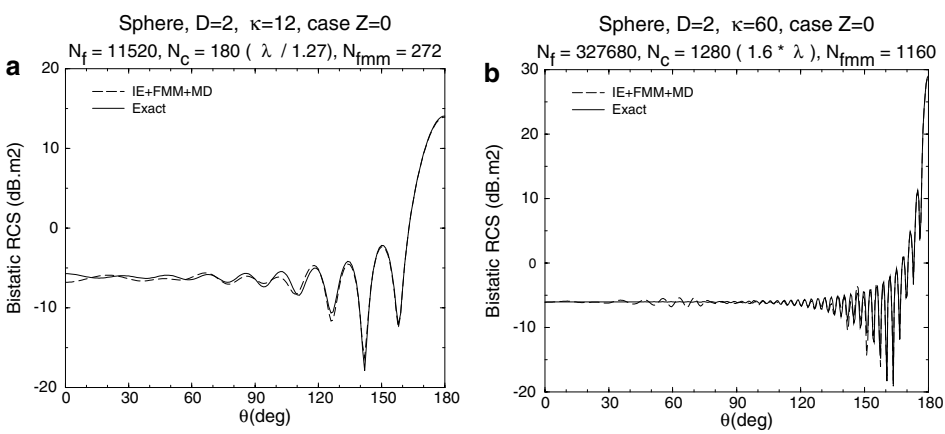

FIG. 12. $\mathcal{C}$(IE + MD + FMM), Neumann case, $\kappa = 12$ or 60. (a) $\kappa = 12$; (b) $\kappa = 60$.

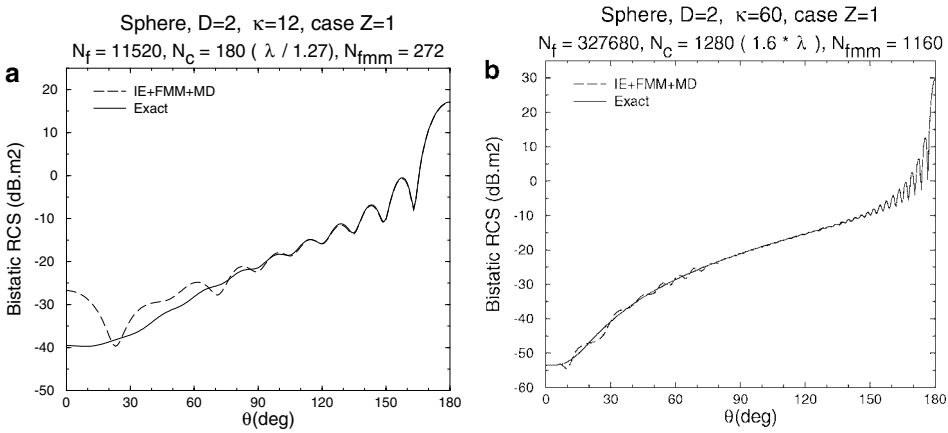

FIG. 13. $\mathcal{C}(\mathrm{IE}+\mathrm{MD}+\mathrm{FMM})$, Robin case, $\kappa = 12$ or 60. (a) $\kappa = 12$; (b) $\kappa = 60$.

of about $\lambda/1.7$. Figure 14 shows the coarse mesh of the Cetaf used for the following tests (see also [13, p. 233]; Fig. 43). The fine mesh consists of 57,504 triangles and the coarse one consists of 3594 triangles. The reference or classical solution was computed with the code $\mathcal{C}(\mathrm{IE}+\mathrm{FMM})$ using the fine mesh, and with a residual criterion of 10^{-3} for GC1. Because of the high CPU cost of the classical solution, we used a residual criterion on of 5×10^{-3} for the GC2. We consider that the solution obtained has sufficiently converged at least for the RCS whose evolution is negligible during the last iterations. The other results were obtained with a residual criterion of 10^{-3} for GC1 and GC2. Moreover, all the results are obtained for the Robin boundary condition. In the following comparisons, we consider the solution obtained with our code $\mathcal{C}(\mathrm{IE}+\mathrm{MD}+\mathrm{FMM})$ and the solution computed with $\mathcal{C}(\mathrm{IE}+\mathrm{FMM})$ using the coarse mesh with an average edge length of about $\lambda/1.7$, and we compare these solutions to the reference one. Table IX shows that our code has requirements that are close to those of $\mathcal{C}(\mathrm{IE}+\mathrm{FMM})$ using the coarse mesh while our code gives a better accuracy than $\mathcal{C}(\mathrm{IE}+\mathrm{FMM})$ using the coarse mesh. The currents shown in Fig. 15 confirm this note. However, the accuracy of the coupling $\mathcal{C}(\mathrm{IE}+\mathrm{FMM}+\mathrm{MD})$ is not sufficient, especially concerning the RCS (see Table IX and Fig. 16a). Here, Err(AD) denotes the relative error in l^2-average made on the diffusion amplitude in comparison with the reference solution. Then, we computed the solution with $\mathcal{C}(\mathrm{IE}+\mathrm{FMM})$ using the fine mesh, initialized with the solution given by our code. In this way, after two iterations of GC2, after about 25 h (including the step of initialization of Table IX), $\mathcal{C}(\mathrm{IE}+\mathrm{FMM})$ gives accurate results with $\mathrm{Err(AD)} = 1.5\times10^{-2}$ (see Fig. 15d and Fig. 16c). In the case of the Cetaf, our new method also proves interesting. It can be used like a good initialization of classical methods. Moreover, the curves in Fig. 16 show two peaks which can be interpreted as Darve did [13]. The first peak occurs for $\theta = 45^\circ + 180^\circ$. This corresponds to the shadow

TABLE VII
Accuracy with the Neumann Boundary Condition

Figure	κ	N_f	N_c	$Y_I X$	Err(AD)
12a	12	11,520	180	2.2×10^{-2}	3.7×10^{-3}
12b	60	327,680	1280	1.2×10^{-2}	2.8×10^{-3}

TABLE VIII
Accuracy with the Robin Boundary Condition

Figure	κ	N_f	N_c	$Y_I X$	Err(AD)
13a	12	11,520	180	1.4×10^{-2}	6.5×10^{-2}
13b	60	327,680	1280	1.8×10^{-3}	3.3×10^{-3}

TABLE IX
$\mathcal{C}$(IE + MD) and $\mathcal{C}$(IE + MD + FMM): Cost and Accuracy

	CPU time	Memory	$Y_I X$	Err(AD)
$\mathcal{C}$(IE + FMM) (λ/7)	200 h	3164 MB	5×10^{-2}	
$\mathcal{C}$(IE + MD + FMM) (λ/1.7)	5 h 23 min	1012 MB	4×10^{-2}	1.7×10^{-1}
$\mathcal{C}$(IE + FMM) (λ/1.7)	1 h 29 min	779 MB	2.9×10^{-1}	2.4×10^{-1}

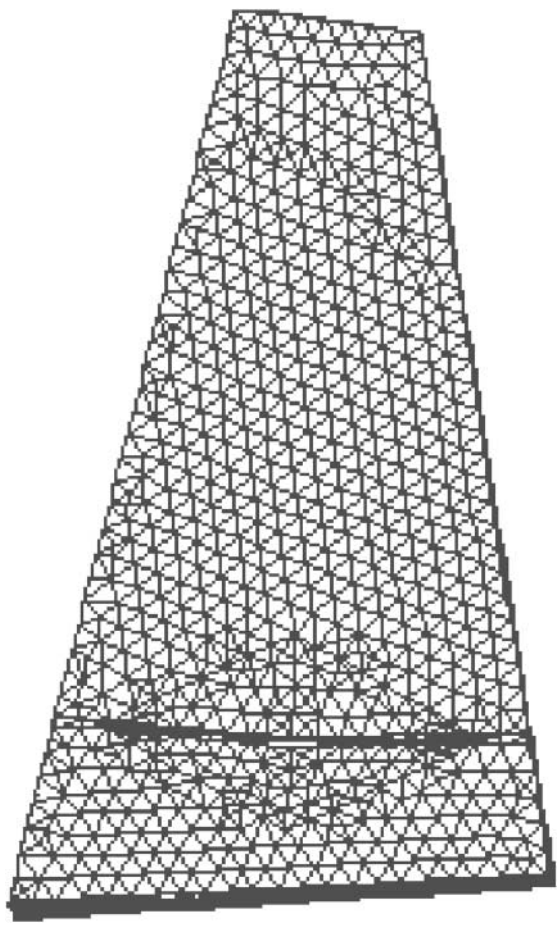

FIG. 14. The coarse mesh of the Cetaf.

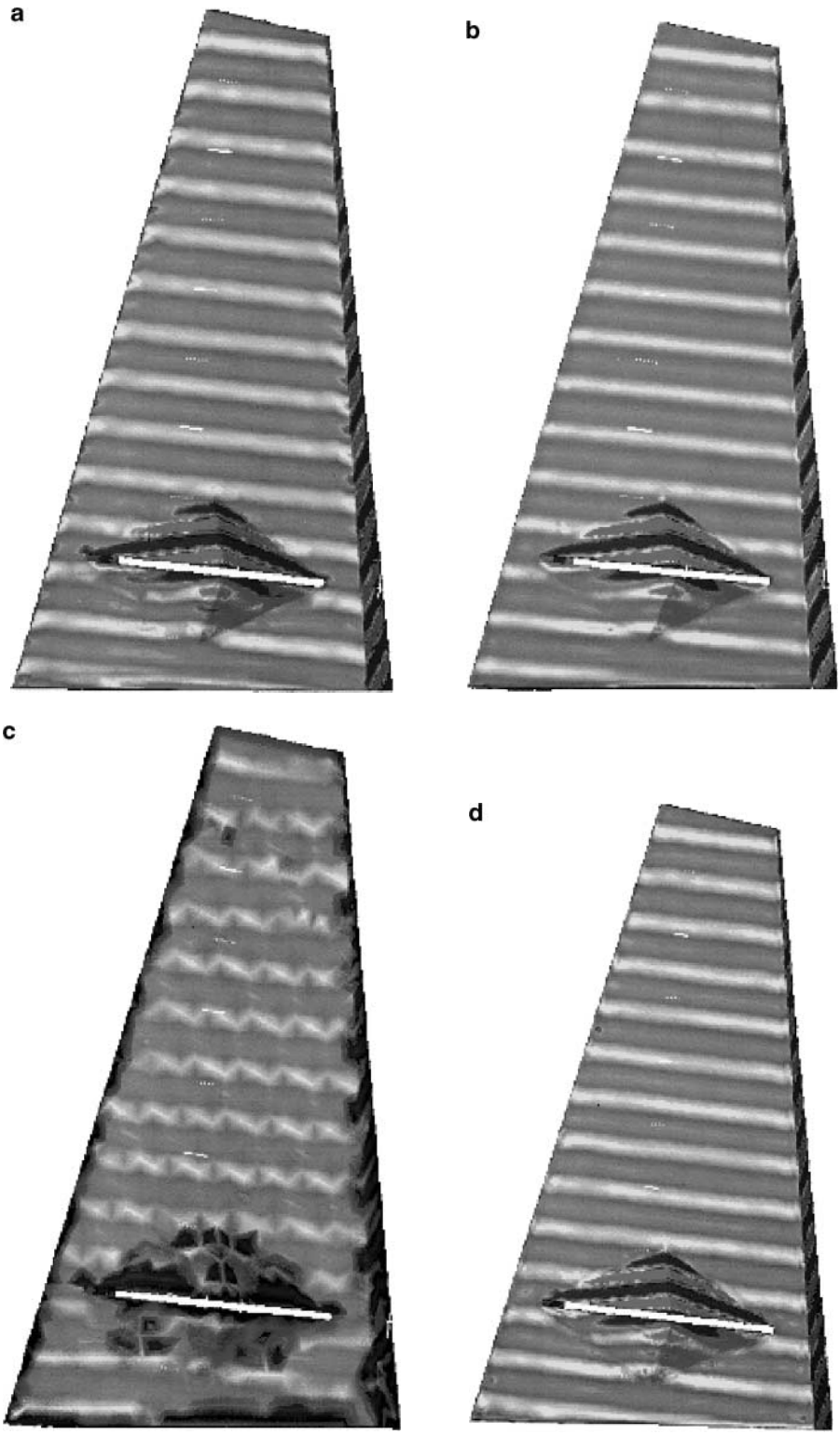

FIG. 15. Real part of the currents on the Cetaf. (a) IE + FMM + MD; (b) IE + FMM($\lambda/7$); (c) IE + FMM($\lambda/1.7$); (d) IE + FMM($\lambda/7$) initialized by (a).

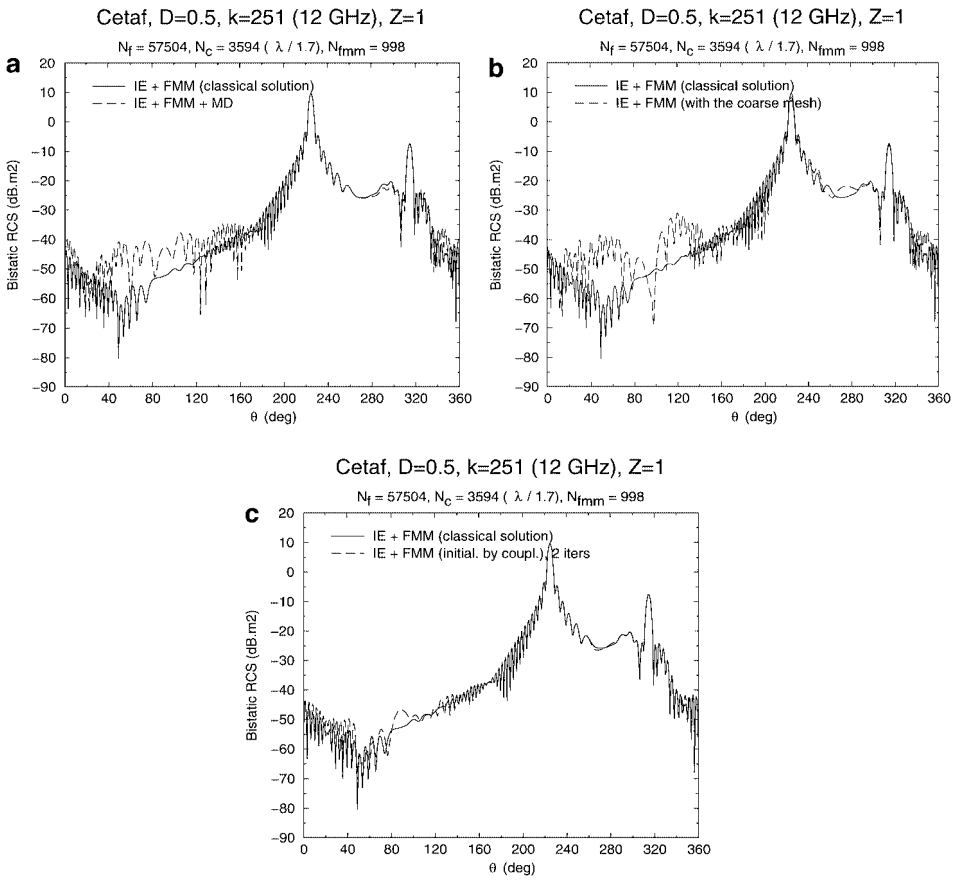

FIG. 16. Bistatic RCS of the Cetaf. (a) IE + FMM(λ/7)/IE + FMM + MD; (b) IE + FMM(λ/7)/IE + FMM(λ/1.7); (c) IE + FMM(λ/7)/IE + FMM(λ/7) initialized.

region. The second one corresponds to a reflection of the incident wave on the surface of the Cetaf. This occurs for $\theta = 45^\circ + 180^\circ + 90^\circ$. Figure 15 also shows the period of the real part of the current already presented by Darve [13].

7. CONCLUSION

The method we have developed couples two kinds of methods in order to speed up the solution of integral equations. First, concepts of the geometrical and physical theories of diffraction enable us to reduce the size of the system considered, using the microlocal discretization introduced by Abboud *et al.* [1, 2]. Second, concepts of the one-level FMM enable us to speed up the calculation of the matrix of the new system. Such a combination has resulted in a new method that is more efficient than the one-level FMM and more robust than the microlocal discretization, which uses the theory of the stationary phase. Moreover, this coupling has been performed within a new formulation of the integral equations which is suitable for iterative resolution.

Numerical tests confirm the relevant reduction of both CPU time and memory cost. We have obtained good accuracy for resolutions based on rather coarse meshes, with an

average edge length of up to two wavelengths. However, both Neumann and Robin cases merit further improvements, considering a piecewise 2-degree polynomial surface in order to approximate the boundary of the object.

Moreover, we are contemplating the coupling with the multilevel FMM, which seems to further reduce the calculation of the matrix of the new system. This should result in an algorithm more efficient than the multilevel FMM, thanks to the approximation of the phase function. For nonconvex objects, we also plan to conduct a study based on the consideration of more directions in the phase approximation, taking our inspiration from the work of A. de La Bourdonnaye. In addition, we will implement the new method within Maxwell's equations [23].

ACKNOWLEDGMENTS

I thank K. Mer-Nkonga, CEA-CESTA, and A. Bachelot, University of Bordeaux I, for their contributions to this work.

REFERENCES

1. T. Abboud, J.-C. Nédélec, and B. Zhou, Méthodes des équations intégrales pour les hautes fréquences, *C. R. Acad. Sci. Paris* **318**, 165 (1994).
2. T. Abboud, J.-C. Nédélec, and B. Zhou, Improvement of the integral equation method for high frequency problems, in *Third International Conference on Mathematical Aspects of Wave Propagation Phenomena* (Soc. for Industr. & Appl. Math., Philadelphia, 1995), p. 178.
3. M. Abramowitz and I. A. Stegun, *Handbook of Mathematical Functions with Formulas, Graphs, and Mathematical Tables* (Wiley, New York, 1972).
4. V. M. Babič and V. S. Buldyrev, *Short-Wavelength Diffraction Theory.* Springer-Verlag, 1991.
5. N. Bartoli and F. Collino, Integral equations via saddle point problem for acoustic problems, *Mod. Math. Anal. Numer.* **34**(5), 1023 (2000).
6. D. Bouche and F. Molinet, *Méthodes Asymptotiques en Électromagnétisme* (Springer-Verlag, Berlin/New York, 1994).
7. W. C. Chew, J. M. Jin, C.-C. Lu, E. Michielssen, and J. M. Song, Fast solution methods in electromagnetics, *IEEE Trans. Antennas Propagation* **45**(3), 533 (1997).
8. R. Coifman, V. Rokhlin, and S. Wandzura, The fast multipole method for the wave equation: A pedestrian prescription, *IEEE Antennas Propagation Mag.* **35**(3), 7 (1993).
9. E. Darrigrand, Fast multipole method and microlocal discretization for the helmholtz equation in three dimensions, in *Second International Conference on Boundary Integral Methods: Theory and Applications* (Inst. of Math. Appl., Southend-on-Sea, 2000).
10. E. Darrigrand, Fast multipole method and microlocal discretization for the 3-D Helmholtz equation, in *2001 IEEE AP-S International Symposium and USNC/URSI National Radio Science Meeting* (IEEE Press, New York, 2001).
11. E. Darve, Fast multipole method: A mathematical study, *C. R. Acad. Sci. Paris* **325**, 1037 (1997).
12. E. Darve, The fast multipole method. I: Error analysis and asymptotic complexity, *SIAM J. Numer. Anal.* **38**(1), 98 (2000).
13. E. Darve, The fast multipole method: Numerical implementation, *J. Comput. Phys.* **160**, 195 (2000).
14. A. de la Bourdonnaye, High frequency approximation of integral equations modelizing scattering phenomena, *Mod. Math. Anal. Numer.* **28**(2), 223 (1994).
15. A. de la Bourdonnaye, Une méthode de discrétisation microlocale et son application à un problème de diffraction, *C. R. Acad. Sci. Paris* **318**, 385 (1994).
16. B. Després, Fonctionnelle quadratique et équations intégrales pour les problèmes d'onde harmonique en domaine extérieur, *Mod. Math. Anal. Numer.* **31**(6), 679 (1997).

17. L. Greengard and V. Rokhlin, The rapid evaluation of potential fields in three dimensions, in *Vortex Methods in Lecture Notes in Mathematics, 1360* (Springer-Verlag, Berlin/New York, 1998), p. 121.
18. L. Greengard and V. Rokhlin, A new version of the fast multipole method for the Laplace equation in three dimensions, *Acta Numer.* **6**, 229 (1997).
19. L. Hörmander, *The Analysis of Linear Partial Differential Operators I* (Springer-Verlag, Berlin/New York, 1983).
20. S. Koc, J. M. Song, and W. C. Chew, Error analysis for the numerical evaluation of the diagonal forms of the scalar spherical addition theorem, *SIAM J. Numer. Anal*. **36**(3), 906 (1999).
21. R. B. Melrose and M. E. Taylor, Near peak scattering and the corrected Kirchhoff approximation for a convex obstacle, *Adv. Math*. **55**, 242 (1985).
22. K. Mer, The fast multipole method applied to a mixed integral system for time-harmonic Maxwell's equations, in *Second International Conference on Boundary Integral Methods: Theory and Applications* (Inst. of Math. Appl., Southend-on-Sea, 2000).
23. K. Mer-Nkonga, The fast multipole method applied to a mixed integral system for time-harmonic Maxwell's equations, in *JEE 02: European Symposium on Numerical Methods in Electromagnetics* (Bas Michielsen and Francine Decavèle, ONERA, Toulouse, 2002), pp. 121–126.
24. J.-C. Nédélec, *Acoustic and Electromagnetic Equations, Integral Representation for Harmonic Problems* (Springer-Verlag, Berlin/New York, 2001).
25. J. Rahola, Diagonal forms of the translation operators in the fast multipole algorithm for scattering problems, *BIT* **36**(2), 333 (1996).
26. V. Rokhlin, Rapid solution of integral equations of scattering theory in two dimensions, *J. Comput. Phys*. **86**(2), 414 (1990).
27. V. Rokhlin, *Diagonal Forms of Translation Operators for the Helmholtz Equation in Three Dimensions*, Research Report YALEU/DCS/RR-894 (Yale Univ., New Haven, 1992).
28. J. M. Song and W. C. Chew, Multilevel fast multipole algorithm for solving combined field integral equations of electromagnetic scattering, *Microwave Opt. Tech. Lett.* **10**(1), 14 (1995).
29. J. M. Song, C.-C. Lu, and W. C. Chew, Multilevel fast multipole algorithm for electromagnetic scattering by large complex objects, *IEEE Trans. Antennas Propagation* **45**(10), 1488 (1997).
30. J. M. Song, C.-C. Lu, W. C. Chew, and S. W. Lee, *Fast Illinois Solver Code (FISC) Solves Problems of Unprecedented Size at the Center for Computational Electromagnetics*, University of Illinois, Research Report CCEM-23-97 (Univ. of Illinois, Urbana Champaign, 1997).
31. B. Stupfel, A hybrid finite element and integral equation domain decomposition method for the solution of the 3-D scattering problem, *J. Comput. Phys.* **172**, 451 (2001).
32. J.-D. Benamov and B. Després, A domain decomposition method for the Helmholtz Equation and related optimal control problems, *J. Comput. Phys.* **136**, 68–82 (1997).
33. M. E. Taylor, *Pseudodifferential Operators* (Princeton Univ. Press, Princeton, NJ, 1981).
34. R. L. Wagner and W. C. Chew, A ray-propagation fast multipole algorithm, *Microwave Opt. Tech. Lett.* **7**(10), 435 (1994).
35. B. Zhou, *Méthode des Équations Intégrales pour la Résolution des Problèmes de Diffraction à Hautes Fréquences*, Thèse de doctorat (Université Paris, 1995).